THE EUROPEAN GRAVITY FIELD AND STEADY-STATE OCEAN CIRCULATION EXPLORER SATELLITE MISSION: ITS IMPACT ON GEOPHYSICS

J. A. JOHANNESSEN[1,2], G. BALMINO[3], C. LE PROVOST[4], R. RUMMEL[5], R. SABADINI[6], H. SÜNKEL[7], C. C. TSCHERNING[8], P. VISSER[9], P. WOODWORTH[10], C. W. HUGHES[10], P. LEGRAND[11], N. SNEEUW[5,12], F. PEROSANZ[3], M. AGUIRRE-MARTINEZ[13], H. REBHAN[13] and M. R. DRINKWATER[13]

[1]*Nansen Environmental and Remote Sensing Center, Edv. Griegsvei 3a, 5059 Bergen, Norway*
[2]*University of Bergen, Geophysical Institute, Allégaten 70, 5007 Bergen, Norway*
[3]*Centre National d'Etudes Spatiales – GRGS, 18 Av. Ed. Belin, 31401 Toulouse, Cedex 4, France*
[4]*Laboratoire d'Etudes en Géophysique et Océanographie Spatiales, 14 Av. Ed. Belin, 31400 Toulouse, Cedex 4, France*
[5]*Technical University of Munich, Astronomical and Physical Geodetic Institute, Arcistrasse 21, 80333 Munich, Germany*
[6]*Dipartimento di Scienze della Terra, Università di Milano, Via L. Cicognara 7, 20129 Milano, Italy*
[7]*Technical University of Graz, Mathematical Geodesy and Geoinformatics, Steyrergasse 30, 8010 Graz, Austria*
[8]*University of Copenhagen, Department of Geophysics, Denmark*
[9]*Delft Institute for Earth-Oriented Space Research, Delft University of Technology, Kluyverweg 1, 2629 HS, Delft, The Netherlands*
[10]*Proudman Oceanographic Laboratory, Bidston Observatory, Bidston Hill, Prenton CH43 7RA, United Kingdom*
[11]*IFREMER, Physical Oceanography Department, BP 70, Technopole Brest Iroise, 29280 Plouzané, France*
[12]*Department of Geomatics Engineering, University of Calgary, 2500 University Drive, Calgary, Alberta, T2N 1N4, Canada*
[13]*European Space Agency - ESTEC, Keplerlaan 1, 2201 AZ Noordwijk, The Netherlands*
E-mail: Johnny.johannessen@nersc.no

(Received 9 July 2002; Accepted 13 May 2003)

Abstract. Current knowledge of the Earth's gravity field and its geoid, as derived from various observing techniques and sources, is incomplete. Within a reasonable time, substantial improvement will come by exploiting new approaches based on spaceborne gravity observation. Among these, the European Space Agency (ESA) Gravity field and steady-state Ocean Circulation Explorer (GOCE) satellite mission concept has been conceived and designed taking into account multi-disciplinary research objectives in solid Earth physics, oceanography and geodesy. Based on the unique capability of a gravity gradiometer combined with satellite-to-satellite high-low tracking techniques, an accurate and detailed global model of the Earth's gravity field and its corresponding geoid will be recovered. The importance of this is demonstrated by a series of realistic simulation experiments. In particular, the quantitative impact of the new and accurate gravity field and geoid is examined in studies of tectonic composition and motion, Glaciological Isostatic Adjustment, ocean mesoscale variability, water mass transport, and unification of height systems. Improved knowledge in each of these fields will also ensure the accumulation of new understanding of past and present sea-level changes.

Surveys in Geophysics **24:** 339–386, 2003.

1. Introduction

As for any other planet, the Earth's geological evolution has resulted in a *gravity* field that departs significantly from an ellipsoid. (Terms in italic are defined in the glossary at the end of the main text.) The differences between the real, measured values of *gravity* and those that would be produced by the idealised ellipsoidal shaped body are denoted as *gravity anomalies*. These anomalies range typically between $\pm$ 300 mGal (1 mGal = 10^{-5} m/s^2), with higher magnitudes in active tectonic areas. They represent a measure of the imbalance in mass between that of the surface topography and the corresponding density contrasts beneath, and can be related to density anomalies in the solid Earth and ultimately to internal stresses and motions.

The *geoid* is a "level surface" which departs from the Earth's idealised 'ellipsoidal shape of equilibrium' by $\pm$ 100 m as a consequence of the topography and density inhomogeneities in the structure of the lithosphere and mantle that result in the *gravity anomalies*. The special significance of the *geoid* is that its shape defines the local horizontal and on land provides the reference surface for topography. Over the ocean it would correspond to the mean sea-level if the surface were at rest.

The primary aim of the Gravity Field and Steady-State Ocean Circulation Explorer (hereafter termed GOCE) Mission approved by the European Space Agency (ESA, 1999) is to provide unique models of the Earth's *gravity* field and of its *equipotential surface* or level surfaces, as represented by the *geoid*, on a global scale with high spatial resolution (100 km) and to very high accuracies (1 mGal and 1 cm). Such an advance in the knowledge of the Earth's *gravity* field and its *geoid* will help to develop a much better understanding of how the Earth's interior system works as schematically illustrated in Figure 1.

New and fundamental insight is therefore expected into a wide range of multidisciplinary research and application areas, including solid Earth physics, oceanography and geodesy. Moreover, such accurate satellite GOCE measurements at a 100 km spatial resolution will, in turn, play an essential role in improving the local gravity field by reducing bias and trend in airborne gravimetry data.

To reach the measurement goal and meet the scientific objectives, the payload consists of an electrostatic gradiometer, a multi-channel GPS receiver, and a laser retroreflector (Drinkwater et al., 2003). GOCE is planned for launch in 2006. It will fly in a Sun-synchronous, circular, dawn-dusk low Earth orbit, with an inclination of 96.5° and altitude of 250 km. The nominal mission duration is 20 months, including a 3 months commissioning and calibration phase and two measurement phases of 6 months duration each separated by a long-eclipse hibernation period.

In this paper we review the background and scientific as well as technical justification for the mission in Section 2. Drawing on these arguments, Section 3 discusses the importance of the research objectives by quantitative demonstration of the usefulness and application potential within the multidisciplinary research fields. Section 4 addresses the mission goal with its specific objectives,

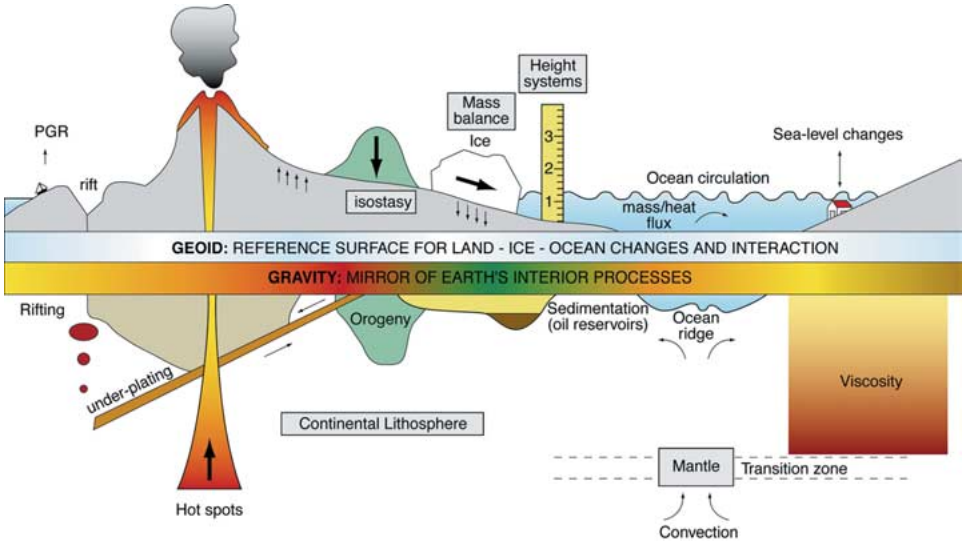

Figure 1. The gravity field as derived by the GOCE mission has a twofold role in the Earth sciences: the geoid as a hypothetical ocean surface at rest (for investigation of ocean circulation, ice, sea-level, height system) and gravity as a "mirror" of processes occurring inside the Earth (rifting, sedimentation, mass readjustment).

and provides a comparison of expected mission performance versus observation requirements based on advanced end-to-end simulation which demonstrates the feasibility of transforming the raw data via calibration and validation to geophysical parameters and data products. In Section 5 we summarize the overall findings.

2. Background and Scientific Justification

Current knowledge of the Earth's *gravity* field and its *geoid*, as derived from various observing techniques and sources, is incomplete. Within a reasonable time, substantial improvement can only come by exploiting new approaches based on satellite *gravity* observation methods. In this section we provide an overview of the rationale that leads from the science case to the proposed mission concept underlying GOCE. For more details on the rationale, readers are referred to Rummel et al. (2001).

2.1. State-of-the-art of gravity field determination

Gravitational acceleration as expressed by Newton's fundamental law of gravitation is a three-dimensional vector field. Its dominating feature reflects the almost spherical shape of the Earth, the well known 9.81 m/s^2. The main deviations are due to the Earth's rotation and oblateness. This section focuses on the importance

of much smaller deviations that are due to the gravitational attractions of a wide range of mass inhomogeneities at the Earth's surface and in its interior.

For global *gravity* field analysis, the Earth's *gravitational potential* coefficients are represented by a fully normalized spherical harmonic series (Heiskanen and Moritz, 1967):

$$V(r,\theta,\lambda) = \frac{GM}{R}\sum_{\ell=0}^{\infty}\left(\frac{R}{r}\right)^{\ell+1}\sum_{m=0}^{\ell}\bar{P}_{\ell m}(\sin\theta)(\bar{C}_{\ell m}\cos m\lambda + \bar{S}_{\ell m}\sin\lambda m\lambda)$$

$$= \frac{GM}{R}\sum_{\ell=0}^{\infty}\left(\frac{R}{r}\right)^{\ell+1}\sum_{m=-\ell}^{\ell}K_{\ell m}Y_{\ell m}(\theta,\lambda) \tag{2.2.1}$$

with $\bar{P}_{\ell m}$ and $Y_{\ell m}$ the real and complex valued spherical harmonics of degree ℓ and order m, respectively, GM the universal gravitational constant (G) times the mass (M) of the Earth, and R the Earth's mean radius. In satellite applications, $\{r, \theta, \lambda\}$ are the spherical co-ordinates of the spacecraft, the origin being at the centre of the Earth. With $r = R + h$ and h the altitude of the satellite, the factor $(R/r)^{\ell+1}$ describes the field attenuation with altitude. The normalised series coefficients $\bar{C}_{\ell m}$ and $\bar{S}_{\ell m}$ (or in complex form $K_{\ell m}$) are to be determined. They are the fundamental *gravity* field unknowns. The infinite series is usually truncated at the maximum resolvable degree $\ell = L$, which can be translated into a corresponding spatial-scale (half-wavelength given in km) D with

$$D = 20000/L. \tag{2.2.2}$$

The series coefficients allow the determination of *geoid heights* (measured in metres above an adopted reference ellipsoid using a spherical approximation) with:

$$N(\theta,\lambda) = R\sum_{\ell=2}^{L}\sum_{m=0}^{\ell}\bar{P}_{\ell m}(\sin\theta)[\Delta\bar{C}_{\ell m}\cos m\lambda + \Delta\bar{S}_{\ell m}\sin m\lambda] \tag{2.2.3}$$

and of *gravity anomalies* (measured in mGal) on the *geoid* surface by

$$\Delta g(\theta,\lambda) = \gamma\sum_{\ell=2}^{L}(\ell-1)\sum_{m=0}^{\ell}\bar{P}_{\ell m}(\sin\theta)[\Delta\bar{C}_{\ell m}\cos m\lambda + \Delta\bar{S}_{\ell m}\sin m\lambda] \tag{2.2.4}$$

where γ is the normal *gravity* (see also Glossary), $\Delta\bar{C}_{\ell m}$ and $\Delta\bar{S}_{\ell m}$ denote the deviation of the spherical harmonic coefficients from those of an elliptical gravity field model.

Alternatively, the *gravitational potential* can be expressed in a set of orbit elements (describing a circular satellite orbit) as

$$V(r,u,\Lambda) = \frac{GM}{R}\sum_{L=0}^{L}\left(\frac{R}{r}\right)^{\ell+1}\sum_{m=-\ell}^{\ell}\sum_{k=-\ell}^{\ell}K_{\ell m}F_{\ell mk}(I)\exp[I(ku + m\Lambda)] \tag{2.2.5}$$

with $F_{\ell mk}$ being the inclination functions (Kaula, 1966), I the orbit inclination, $\Lambda = \Omega - \theta_G$ the longitude of the ascending node (where Ω is the right ascension of the ascending node, and θ_G the Greenwich sidereal time), and u the argument of latitude of the satellite (in plane longitude measured from the ascending node).

From the *gravitational potential*, any other *gravity* function can be deduced quite easily. This includes *geoid heights* (Equation (2.2.3)), *gravity anomalies* (Equation (2.2.4)) and the gravitational acceleration vector. For gradiometry, second-order derivatives (with respect to the three spatial directions), the so-called gravitational gradients, are of particular interest. The nine second-order derivatives form a symmetric 3×3 matrix where the trace (diagonal) is zero in empty space. For example, the radial component of the gravitational gradient can be expressed as:

$$V_{zz} = \frac{\partial^2 V}{\partial z^2} = \frac{GM}{R} \sum_{\ell=0}^{L} \frac{(\ell+1)(\ell+2)}{R^2} \left(\frac{R}{r}\right)^{\ell+3} \times \sum_{m=-\ell}^{\ell} \sum_{k=-\ell}^{\ell} K_{\ell m} F_{\ell mk}(I) \exp[I(ku + m\Lambda)] \tag{2.2.6}$$

In this expression it is important to note that, to a large degree, the "differentiation factor" $(\ell + 1)(\ell + 2)$ can counteract the attenuation factor $(R/r)^{\ell+3}$. The corresponding expressions for orbit perturbations Δx, Δy and Δz in the along-track, cross-track and radial directions and those for all second derivatives of the *gravitational potential* are summarised in Table I. The orbit perturbations are based on a linear perturbation theory, particular solution (Kaula, 1966; Rosborough, 1987).

In the case of Δy, V_{xy} and V_{yz} a modified inclination function has been used; it is not essential to use modified inclination functions, it is merely handy to do so. An alternative is to use derivatives of the "conventional" inclination functions (Sneeuw, 1992). The parameter $\beta = (k\dot{u} + m\dot{\Lambda})/n$ is the normalised frequency of the perturbation, with n the mean orbit frequency.

In *gravity* field studies the average signal strength (i.e. the power spectrum) is expressed in terms of degree variances c_λ, where

$$c_\ell = \sum_{m=0}^{\ell} [\bar{C}_{\ell m}^2 + \bar{S}_{\ell m}^2] = \sum_{m=-\ell}^{\ell} |K_{\ell m}|^2 \tag{2.2.7}$$

or in terms of their square roots divided by $(2\ell + 1)$, the root-mean-square (r.m.s.) value per degree. It can be shown that on the Earth's surface the degree variances follow *Kaula's rule* of thumb, according to Kaula (1966):

$$c_\ell = 1.6 \frac{10^{-10}}{\ell^3} \quad \text{(dimensionless)} \tag{2.2.8}$$

TABLE I

Sensitivity coefficients (without the common term GM/R) that relate observable orbit perturbations and gradiometric components to the unknown spherical harmonic coefficients (e.g., compare with Equation (2.2.6)). The expressions are given for the along-track, cross-track and radial perturbations, Δx, Δy and Δz, respectively, that can be measured by satellite-to-satellite tracking, and for the second derivatives V_{xx}, V_{yy}, V_{zz}, V_{xy}, V_{xz}, V_{yz}, measurable by satellite gradiometry. Each of these quantities gives a characteristic "view" of the Earth's gravitational field. Also shown (in the two right columns) are the order of magnitudes of the gradiometer components normalized by 1 E (DC value in Eötvös Units, with 1 $E = 10^{-9}$ s^{-2}), i.e., the average size of each of the components, and the average ratio of the individual signal spectral powers with respect to that of the dominant radial component V_{zz}

Observed variable	Sensitivity coefficient	Attenuation coefficient	Order magnitude	Ratio to V_{zz}
Δx	$i\dfrac{2(\ell+1)\beta - k(\beta^2+3)}{\beta^2(\beta^2-1)n^2R}$	$\left(\dfrac{R}{r}\right)^{\ell+2}$		
Δy	$\dfrac{1}{(1-\beta^2)n^2R}$	$\left(\dfrac{R}{r}\right)^{\ell+2}$		
Δz	$\dfrac{(\ell+1)\beta - 2k}{\beta(\beta^2-1)n^2R}$	$\left(\dfrac{R}{r}\right)^{\ell+2}$		
V_{xx}	$\dfrac{-(k^2+\ell+1)}{R^2}$	$\left(\dfrac{R}{r}\right)^{\ell+3}$	−1400/E	3/8
V_{yy}	$\dfrac{k^2-(\ell+1)^2}{R^2}$	$\left(\dfrac{R}{r}\right)^{\ell+3}$	−1400/E	3/8
V_{zz}	$\dfrac{(\ell+1)(\ell+2)}{R^2}$	$\left(\dfrac{R}{r}\right)^{\ell+3}$	2800/E	1
V_{xy}	$\dfrac{ik}{R^2}$	$\left(\dfrac{R}{r}\right)^{\ell+3}$	Small	1/8
V_{xz}	$\dfrac{-ik(\ell+1)}{R^2}$	$\left(\dfrac{R}{r}\right)^{\ell+3}$	≈10/E	1/2
V_{yz}	$-\dfrac{\ell+2}{R^2}$	$\left(\dfrac{R}{r}\right)^{\ell+3}$	Small	1/2

i.e., the field strength tapers off as $1/\ell^3$. At satellite altitude, this attenuation effect is increased by the $(R/r)^{\ell+1}$ term. For high-resolution *gravity* field determination by satellite the main goal and challenge is to counteract this attenuation term, which can be accomplished by using the concept of gradiometry.

2.2. Available gravity data for global gravity fields model

Hitherto three *gravity* data sources have generally been available, namely mean *gravity anomalies*, satellite altimetry and satellite orbit tracking observations. Mean *gravity anomalies*, taken typically over areas of 100×100 km^2 or 50×50 km^2, are derived from terrestrial gravimetry in combination with height measurements and from ship-borne gravimetry. Their accuracy depends on data density and the precision of the height and *gravity* measurements. Before the late 1980s, mean values of acceptable accuracy were available only for North America, Western Europe and Australia. In recent years, due to an enormous effort to encourage data exchange, the situation has significantly improved. However, due in particular to the sparseness of data in some large continental areas and the generally poor quality of older sea gravimetry data, severe inconsistencies remain and the *geoid* precision does not fall much below approximately 50 to 80 cm in most parts of the world.

In ocean areas, satellite altimetry can in some sense be regarded as a direct *geoid* measuring technique. However, after removing time-varying effects, such as tides, by averaging repeated measurements, the resulting stationary sea-surface still deviates from the *geoid* due to dynamic ocean topography. In fact, this difference, the mean-sea-surface topography, is of key importance in oceanography.

For more than three decades now, several institutions have determined geopotential models from satellite orbit tracking observations. These are derived from the combined analysis of orbit tracking of a large number of mostly non-geodetic satellites with different orbit elements. They exploit a variety of tracking techniques, primarily laser and Doppler measurements. These models are presented as sets of coefficients $\bar{C}_{\ell m}$ and $\bar{S}_{\ell m}$ of a spherical harmonic expansion of the field and they provide information on the long wavelength part of the spectrum only. A representative example of one of the best currently available geopotential models, based purely on satellite orbit analysis (no altimetry, no terrestrial surface *gravity*), is the GRIM-4S *gravity* field model (Schwintzer et al., 1997). GRIM-5S which has recently become available is much better than GRIM-4S (Biancale et al., 2000). It is complete to degree $\ell = 72$ and order $m = 72$ (at the higher degrees and order up to 99 only selected, resonant, terms have been included). This corresponds to a spatial half wavelength of $D = 300$ km.

Combined models of these three data sources exist, of which a state-of-the-art model is the EGM96 (Lemoine et al., 1998). However, none of the above three data sources nor their combination can meet the requirements for solid-Earth physics, oceanography and geodesy, even to a limited extent. The solution to this problem must therefore come from dedicated *gravity* field mapping by satellite.

2.3. High-resolution gravity field determination from space

Four fundamental criteria arise for a dedicated satellite *gravity* mission including:

– Uninterrupted tracking in three spatial dimensions

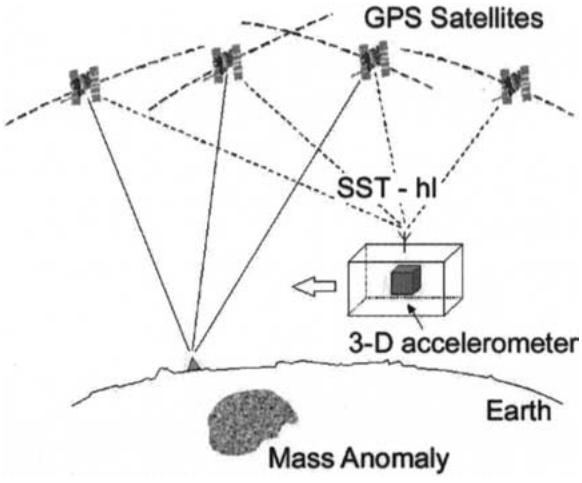

Figure 2a. Concept of satellite-to-satellite tracking in the high-low mode (SST-hl). A low Earth orbiter is tracked by the high orbiting GPS satellites, relative to a net of ground stations. Non-gravitational forces on the low orbiter are measured by accelerometry.

– Measurement or compensation of the effect of non-gravitational forces
– Orbital altitude as low as possible
– Sufficient sensitivity to counteract *gravity* field attenuation at altitude.

The first three criteria can be met by exploiting the concept of satellite-to-satellite tracking in the high-low mode (SST-hl). Thereby a low Earth orbiter (LEO) is equipped with a receiver of the U.S. Global Positioning System (GPS) and with a three-axis accelerometer (see Figure 2a). The receiver "sees" up to twelve GPS satellites at any time. Their ephemerides are determined very accurately by the large network of ground stations that participate in the International GPS Service (IGS). Taking their orbits and the GPS measurements of the LEO (pseudo-range and carrier phase), the orbit of the LEO can be monitored to the few cm-precision level without interruption and in three dimensions (Visser and IJssel, 2000).

The accelerometer at the satellites' centre of mass can measure the non-gravitational forces. The effect of the latter can then be taken into account in the *gravity* reduction, or can be fed to and compensated by a drag-free control mechanism. The first satellite of this type (without drag-free control) is the German CHAMP (Reigber et al., 1996) that was launched on July 15, 2000. However, even with this configuration and with an altitude as low as 300 or 400 km, the problem of *gravity* field attenuation prohibits the attainment of really high-spatial-resolution. Thus, the fourth criterion enters.

The classical approach of highlighting the effect of small- scale features in physics is by differentiation. Two alternative concepts of differentiation can be conceived. Either one applies satellite-to-satellite tracking in the low-low mode (SST-ll) or satellite gradiometry, both combined with SST-hl. In the case of SST-ll (see Figure 2b), two spacecraft essentially in the same orbit and at a distance

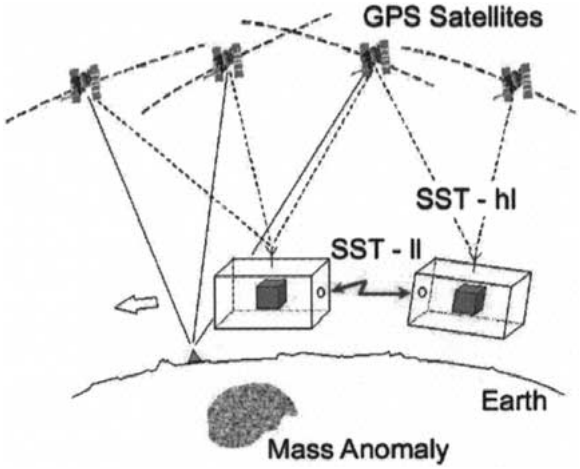

Figure 2b. Concept of satellite-to-satellite tracking in the low-low mode (SST-ll) combined with SST-hl. The relative motion between two low orbiters following each other in the some orbit at a distance of a few hundred kilometres is measured by an inter-satellite link.

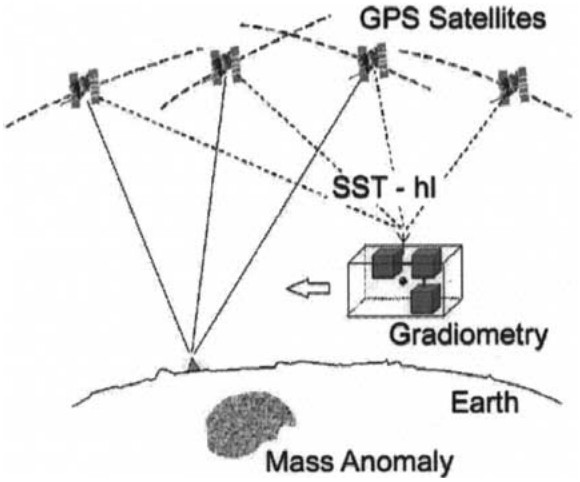

Figure 2c. Concept of satellite gradiometry combined with SST-hl. The second-order derivative of the gravitational potential of the Earth is measured in a low orbiting satellite by differential accelerometry.

of somewhere between 100 and 400 km apart, "chase" each other. The relative motion between the two satellites is measured with the highest possible precision. Again the effect of non-gravitational forces on the two spacecraft can either be compensated for or be measured. The quantity of interest is the relative motion of the centres of mass of the two satellites, which has to be derived from the inter-satellite link together with the measured acceleration and attitude data. The first experiment of this type is the US-German mission GRACE (GRACE, 1998) which was launched in March 2002.

The alternative to SST-ll is to apply satellite gradiometry as proposed for GOCE. Satellite gradiometry is the measurement of acceleration differences, ideally in all three spatial directions, between the test-masses of an ensemble of accelerometers inside one satellite (see Figure 2c). The measured signal is the difference in gravitational acceleration at the test-mass locations inside the spacecraft, where of course the gravitational signal stems from all the attracting masses of the Earth, ranging from mountains and valleys, via ocean ridges, subduction zones, mantle inhomogeneities down to the core-mantle-boundary topography (plus third body perturbations, tides, etc., which have to come from external models or have to be estimated simultaneously). The technique can resolve all these features as they appear in the *gravity* field. The measured signals correspond to the gradients of the component of *gravity* acceleration or, in other words, to the second derivatives of the *gravitational potential*. Non-gravitational acceleration of the spacecraft (for example due to air drag) affects all accelerometers inside the satellite in the same manner and, ideally, drops out when taking the differences. Rotational motion of the satellite does affect the measured differences, but can be separated from the gravitational signal by separating the measured 3×3 matrix of second derivatives into a symmetric and an anti-symmetric part. Again, a low orbit implies relatively large signals.

Generally speaking, one can now argue that the basic observable in the three cases discussed (namely SST-hl, SST-ll and satellite *gravity* gradiometry (SGG)) is *gravitational acceleration* (Balmino et al., 1999). With the orbits of the high-orbiting GPS satellite assumed to be known with high accuracy, the case of SST-hl corresponds to an in-situ 3-D position, velocity or acceleration determination of a LEO. For SST-ll, the principle corresponds to the line-of-sight measurement of the range, range rate or acceleration difference between the two low-orbiting satellites. Finally, in the case of satellite gradiometry, the measurement is of acceleration differences in 3-D over the short baseline of the gradiometer instrument.

In all three cases, the measurement of accelerations plays a crucial role. In the case of SST-hl and SST-ll, accelerometer measurements are required to separate, after integration, the contributions of non-conservative and gravitational accelerations to the (relative) orbital motion of the satellite(s) in terms of position and/or velocity. In the case of gradiometry, the observables are differential accelerometer measurements. In Figure 3 the expected performances of the three measurement techniques are compared relative to the spherical harmonic degree.

CHAMP is to be seen as a pioneer mission, as it is the first time that uninterrupted three-dimensional high-low tracking has been combined with 3-D accelerometry. This technique will not improve our available *gravity* field models dramatically in terms of accuracy and spatial resolution (see line SST-hl in Figure 3), but it will de-correlate the *spherical harmonic coefficients* $\bar{C}_{\ell m}$ and $\bar{S}_{\ell m}$ significantly and therefore make current models much more reliable.

GRACE is the first SST-ll mission. It will improve the accuracy of the *spherical harmonic coefficients* at long and medium spatial-scales by up to three orders of

magnitude. This will allow the measurement of temporal variations in the *gravity* field, such as those due to seasonal and annual variations in groundwater and soil-moisture levels, changes in the masses of the Antarctic and Greenland ice sheets, changes in water mass properties and atmospheric pressure changes (see NRC, 1997). The high slope of the noise line of GRACE (Figure 3) suggests that any decrease or increase of mission performance has little effect on its spatial resolution, but a large effect on its ability to resolve temporal variations.

GOCE will be the first SGG mission. By employing gradiometry, a much flatter noise line is obtained, the slope is roughly decreased by a factor of l-squared (l^2) as compared with the case of SST-hl (Figure 3), leading to a much higher spatial resolution. Here an increase in mission performance has only a minor effect in terms of temporal resolution, but a large effect on its ability to resolve spatial variations. One can expect that *gravity* signatures as short as 65 km will be resolved with GOCE. Thus it is concluded that the two missions, GRACE and GOCE, are complementary, with GRACE focusing in particular on the temporal variations of the *gravity* field and GOCE on attaining maximum spatial resolution.

In summary, GOCE is capable of meeting all of the four fundamental criteria described above, notably:

- It will be continuously tracked in three dimensions by the systems of GPS satellites, relative to the dense ground network of IGS stations
- It will control drag forces and eliminate remaining residual effects by differential measurement, the so-called common mode rejection (CMR) principle. Rotational motion will also be controlled, and remaining rotational effects will be determined by a novel combination of measured off-diagonal gradient components and star sensors (Aguirre-Martinez, 1999)
- It will fly in an extremely low and almost polar orbit (Sun-synchronous)
- It will efficiently overcome the problem of the attenuation of the *gravity* field at altitude by the principle of gradiometry.

In addition, gradiometry has the unique and important ability of being able to measure the gravity field in three spatial dimensions independently and without any preferred direction. It therefore permits observations of the *gravitational field* of the Earth in three complementary "illuminations" with no directional bias and aliasing of any component of the *gravity* field into another component.

3. Expected Impact of the GOCE Mission

The scientific objectives of the GOCE Mission are based on the unique capability of a *gravity* gradiometer to provide an accurate (1mGal and 1 cm) and detailed (better than 100 km resolution) *global model* of the Earth's *gravity* field. This model will, in turn, serve the following multi-disciplinary scientific objectives:

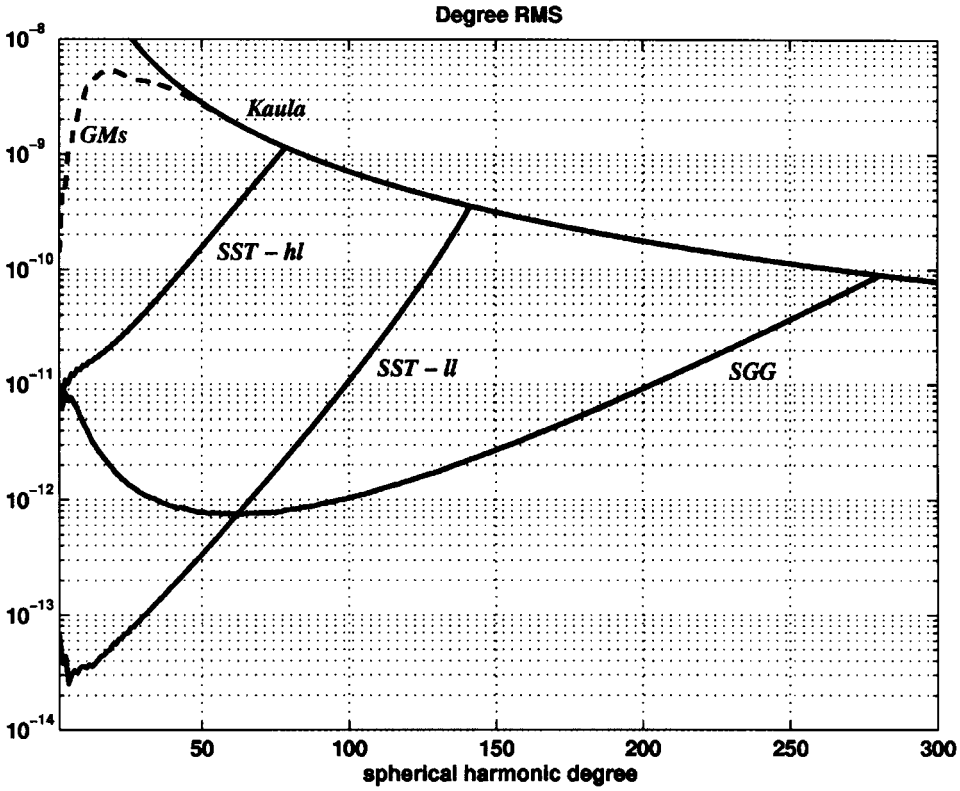

Figure 3. Comparison of expected performances of CHAMP, GRACE and GOCE after Balmino et al. (2001). Representative error degree variance spectra of the gravity mission concepts satellite-to-satellite tracking high to low (SST-hl), SST-ll and satellite gradiometry in comparison with one of the best currently available satellite gravity models (GMs) and with the signal degree variances of the gravity field (Kaula, 1966). The high precision of SST-ll at long and medium length scales and the high-spatial-resolution of gradiometry are apparent here. The signal degree r.m.s. values according to Kaula's rule (Equation (2.2.8)) and the noise degree r.m.s of the best available satellite gravity model intersect somewhere between $\ell = 20$ and $\ell = 30$ ($D \approx 1000$–660 km).

- Solid Earth – to provide new understanding of the physics of the Earth's interior, including geodynamics associated with the lithosphere, mantle composition and rheology, uplifting and subduction processes
- Oceanography – to provide, for the first time, a precise estimate of the marine *geoid*, needed for the quantitative determination, in combination with satellite altimetry, of absolute ocean circulations and their transport of heat and other properties
- Geodesy – to provide a better global height reference system for datum connection, which can serve as a tool to connect the reference surface for the study of topographic processes, including the evolution of ice-sheets and land-surface topography, and the study of the relative levelling of distant tide gauges.

Advances in each of these areas of research will benefit developments in the others, and will also contribute to studies and monitoring of global sea-level change.

Based on reliable and precise quantitative knowledge of the simulated recovery of the *gravity* and *geoid* error characteristics (see Section 4), impact simulation studies have been performed to investigate the expected role of GOCE for these multi-disciplinary areas of scientific research and application.

3.1. SOLID EARTH

A simplified picture of an interior section through the centre of the Earth, inferred from geophysical studies, is shown in Figure 4. The mechanically stiff outer layer is the lithosphere, which is, in turn, subdivided into an oceanic and a continental part. The major geodynamical processes that involve the oceanic lithosphere are spreading at the ocean ridges and subduction at active continental margins. The cold, dense oceanic lithosphere enters the mantle at subduction zones, interacting with the overriding lithosphere, where complicated geodynamical processes, such as back arc opening and volcanism occur. The arrow at the subduction zone indicates the velocity of the plate with respect to the mantle, controlled by the downward pull exerted by the cold subducted plate, the push at the ocean ridge and the basal viscous drag.

The continental lithosphere is the location of the periodic glaciation and deglaciation events, at least during the last million years. The last deglaciation ended about 7000 years ago, and the planet is still recovering its isostatic equilibrium after the unloading of the lithosphere due to the melting of the ice-sheets. The response of the planet to these events (stresses) and the associated *gravity anomalies* depends on crustal and mantle rheologies and lithosphere thickness. This process is termed Post-Glacial Rebound (PGR). A major issue related to the structure of the continental lithosphere is the possible existence of deep roots beneath the continents. Deformation of the continental lithosphere under the influence of extensional forces is visible as elongated depressions called rifts that are present in a variety of tectonic environments.

Rheology studies are important for improving our comprehension of mechanisms that involve the mantle, the portion of the planet beneath the lithosphere down to the core mantle boundary. Mantle convection, depicted by the arrows, is certainly one of these, involving the circulation of mantle material on geologic time-scales. The dynamics of fast upwelling plumes in the mantle that are responsible for the appearance of hot spots in the lithosphere is also important for these studies.

3.1.1. *Joint Use of Spaceborne Gravity and Seismic Data*

Figure 5 shows an example of a simulation over the lithosphere and upper mantle, for a subduction zone for which the structure is sought in terms of slowness anomalies (anomalies in the inverse of the P-wave velocities, related to the square root of the material density). The study results are based on numerical experiments using

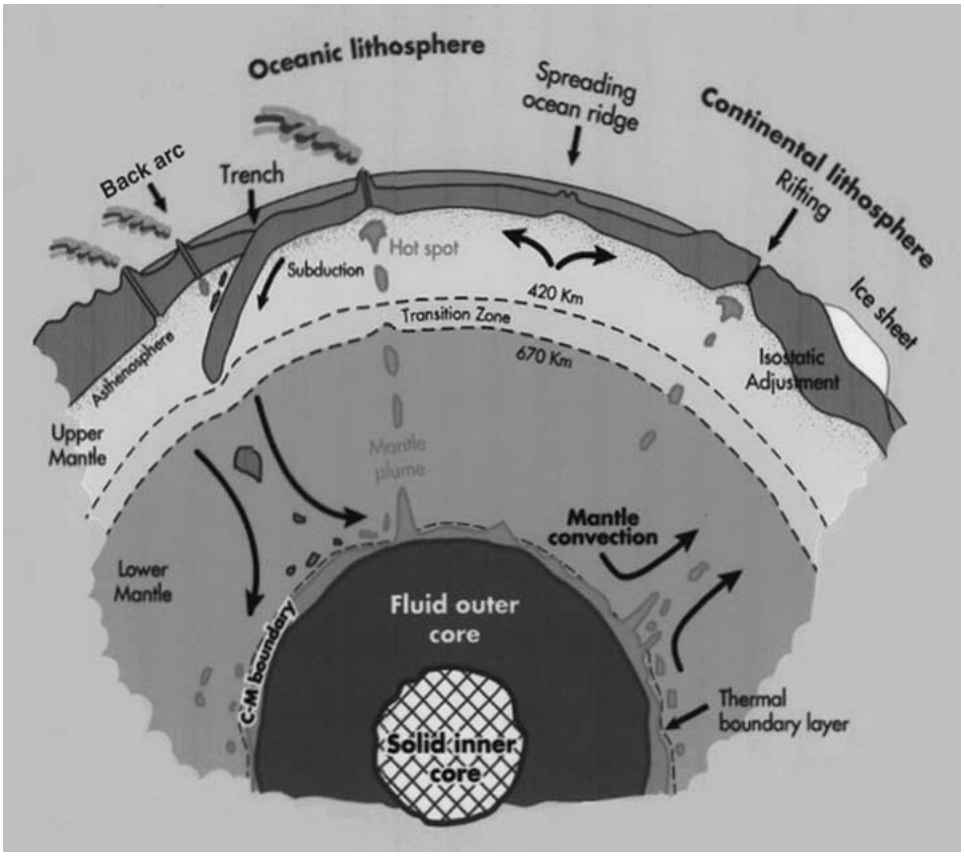

Figure 4. The major dynamic processes of plate tectonics and the layers into which the Earth is differentiated (not to scale). The outer lithosphere, divided into ocean and continental parts, the upper mantle, the transition zone and the lower mantle are shown. The fluid outer core and solid inner core are also portrayed. From left to right, subduction and related back arc opening, hot spots and a spreading ocean ridge are shown. For the continental lithosphere, isostatic adjustment following post-glacial rebound is suggested.

a 2D-model, representing a vertical cross-section of the upper-mantle (Zerbini et al., 1992). The region is partitioned into a set of 150 km $\times$ 60 km cells. The basic slowness field is assumed to be vertically stratified, consistent with the seismic model PREM (Dziewonski and Anderson, 1981). The slab-like structure, reasonably similar to that which exists in the Hellenic arc area, is responsible for negative slowness anomalies in the range -1% to -3% and to the local variation of *gravity anomalies* (50 to 100 mGals over distances of 100 to 300 km). These results, with and without *gravity gradient* observable at GOCE altitude, demonstrate the impact of the *gravity* field information on the quality of the inversion process. The image of the slab is relatively poor when using seismic data alone, while the inclusion of the GOCE data significantly improves the quality of the image of the slab in

both the upper and lower mantle. By varying the parameters of such simulations to determine the sensitivity to *gravity* field knowledge, the required accuracy and resolution are found to be 1 to 2 mGal and 100 km, respectively.

These findings clearly indicate that the joint use of the *gravity anomaly* field retrieved from GOCE and seismic tomography data is extremely promising for detailing the image of the density contrasts within the lithosphere and upper mantle. The combination of the anomalous density contrasts based on GOCE and seismic tomography, of the displacement measurements made at the Earth surface, sensitive to deep seated density anomalies, and of the results of laboratory or theoretical studies on the physical properties of mantle material, will provide major advancements in our understanding of the structure and dynamics of the outermost part of our planet.

As suggested in Figure 5 we can expect to improve the interpretation of signals associated with seismic hazards. Earthquakes can be characterised on at least two time scales: a short one associated with the rupture of a fault and the propagation of elastic waves, and a long one associated with the slow build up of stress due to geodynamic processes and stress relaxation due to visco-elastic flow of the crust and mantle. The GOCE mission will recover the density structure at the upper-mantle level, which is crucial to the modern approach to seismic hazard studies. Results obtained by Negredo et al. (1999) indicate the major impact of lateral variations, in the density structure of the lithosphere and upper mantle, in controlling the stress pattern in an earthquake prone area. It is well known that statistical approaches based on historical records of seismicity are insufficient to mitigate seismic risk, as the slow time scales of earthquakes due to tectonic loading can be several thousands of years, beyond the scope of historical seismic records. A new appraisal in the field of seismic hazard prediction can be gained by modelling the slow build up of stress due to tectonic loading and by comparing with the predicted deformation pattern obtained from GPS surveying.

Such modelling requires knowledge of the density anomalies in the lithosphere and upper mantle, which petrology and seismic tomography alone cannot provide. Only from the inversion of the *gravity* data from GOCE will it be possible to derive the worldwide pattern of the density structures in the uppermost portion of the planet with sufficient accuracy and spatial resolution. These data in turn will advance our understanding of their impact, together with the relative motions of the plates and the rheology of the crust, in controlling earthquake nucleation in seismogenic regions.

3.1.2. *Interpretation of Glacial Isostatic Adjustment*

In order to appreciate the impact of GOCE on the understanding of the physics underlying the Glacial Isostatic Adjustment (GIA) process associated with PGR and on the interpretation of the related solid Earth signals, we compare the worldwide free air *gravity anomalies* having two different spectral contents, the first for spherical harmonics summed from $\ell = 2$ to $\ell = 80$, and the second for a

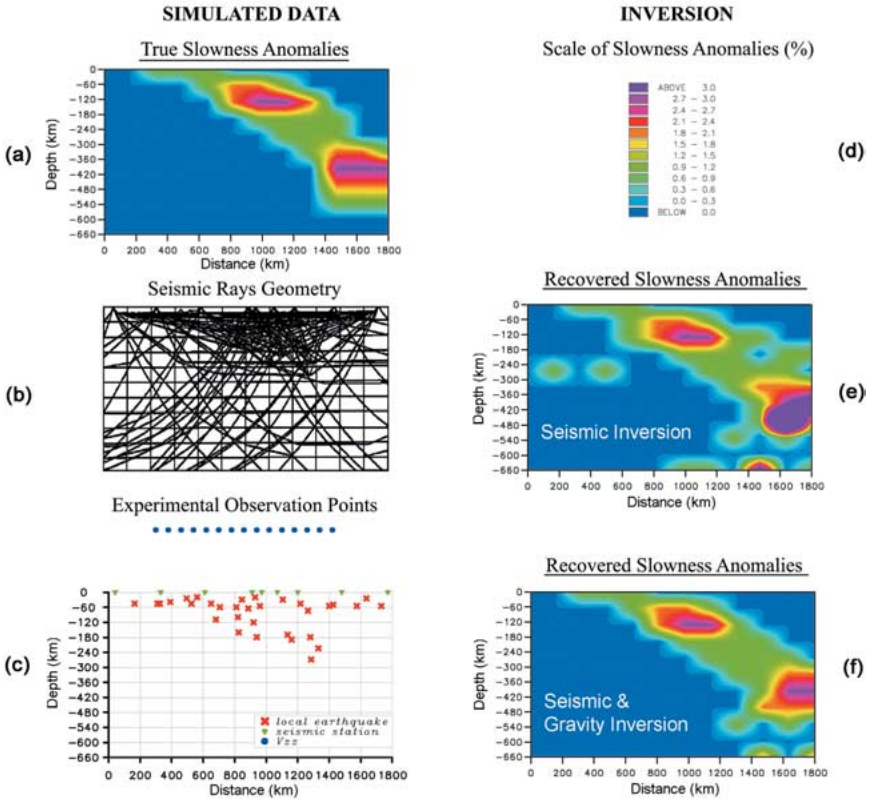

Figure 5. Simultaneous inversion of gravity and seismic tomography data. The left column gives the parameters of the simulation: (a) generated slowness anomalies (equivalent to density anomalies), (b) seismic observables (300 P-wave travel times and seismic rays, observed from 9 surface seismic stations; the rays are radiated by the local earthquakes as well as by rays coming from 5 teleseismic earthquakes which occurred outside the region but which were detected by the seismic stations considered, (c) location of seismic stations (green), of 32 local earthquakes (red), and of 15 measurements of gravity gradients at GOCE satellite altitude (blue). The right column shows (d) legend and colour scale used in inversions of the original slowness anomalies, (e) recovered anomalies using seismic data only, and (f) recovered anomalies using both seismic and gravity data. Seismic travel times have a 5% noise nlevel and the gradiometric data a 5 mE noise level.

summation running from $\ell = 80$ to $\ell = 200$, Figures 6 and 7, respectively. These two cases are chosen in such a way as to compare the potential contributions of GRACE and GOCE on the interpretation of the GIA data. The results are based on a 31-layer Earth viscoelastic model (Vermeersen and Sabadini, 1997), while the loading history is based on the ICE-3G ice model (Tushingam and Peltier, 1991). The lithospheric thickness is 120 km, while the viscosity in the lower mantle is kept fixed at 10^{21} Pa s (Pascal second). The negative peaks displayed in the deglaciated regions are due to the mass deficit following the disintegration of the ice com-

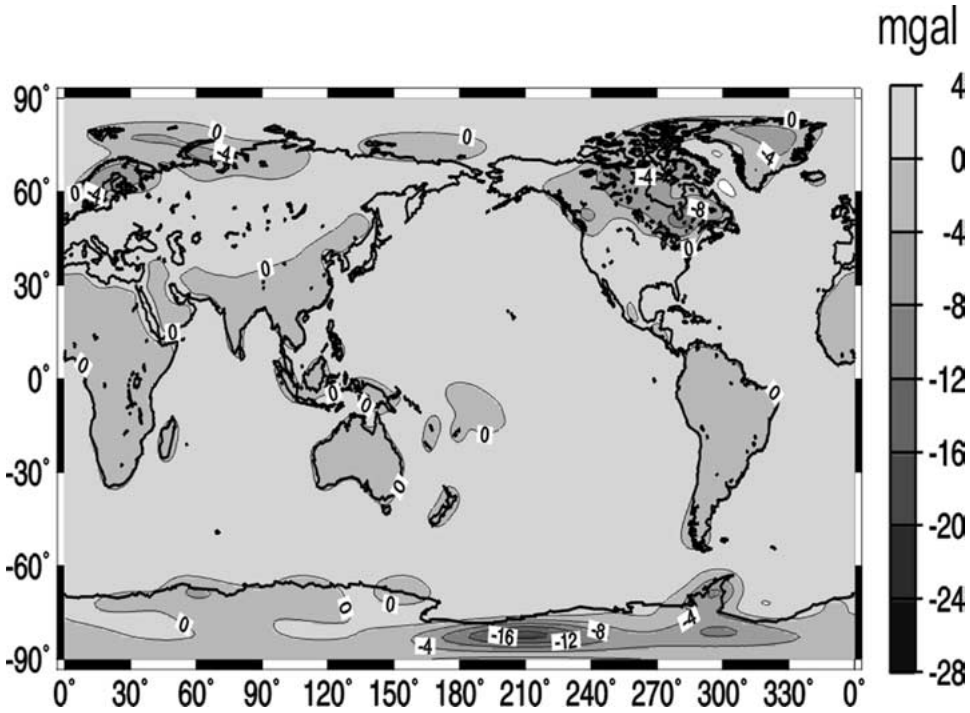

Figure 6. Global map of the modelled present day free air gravity anomaly (mGal) due to Pleistocene deglaciation, for spherical harmonic coefficients in the degree range l = 2–80. The contour interval is 4 mGal.

plexes during the Pleistocene, not completely recovered by the ongoing process of isostatic adjustment.

Figure 6 shows the free air *gravity* map, contributed by GIA, as we expect it will be seen by GRACE, i.e. at lower degree and orders. The largest signals are visible in the deglaciated regions, in North America, with a maximum of −8 mGal, in Northern Europe, with −4 mGal, and in Antarctica, with −16 mGal. If we compare these findings with Figure 7, it is noticeable that the small scale content of the GIA, expected to be visible by GOCE, is about a factor four lower, with the highest signals in Antarctica of −3 mGal; and −2 and −1 mGal respectively in North America and Northern Europe. These results clearly show that about 20–25% of the *gravity anomalies* due to GIA are only likely to be detected by GOCE, which indicates that this mission will play a crucial role in improving our understanding of the physics of GIA, in particular at short wavelengths where the flexural properties of the lithosphere influence the type of deformation and local sea-level records. The location of the *gravity anomalies* near coastal areas suggests that GOCE will play a crucial role in the interpretation of the secular trends in relative sea-level data.

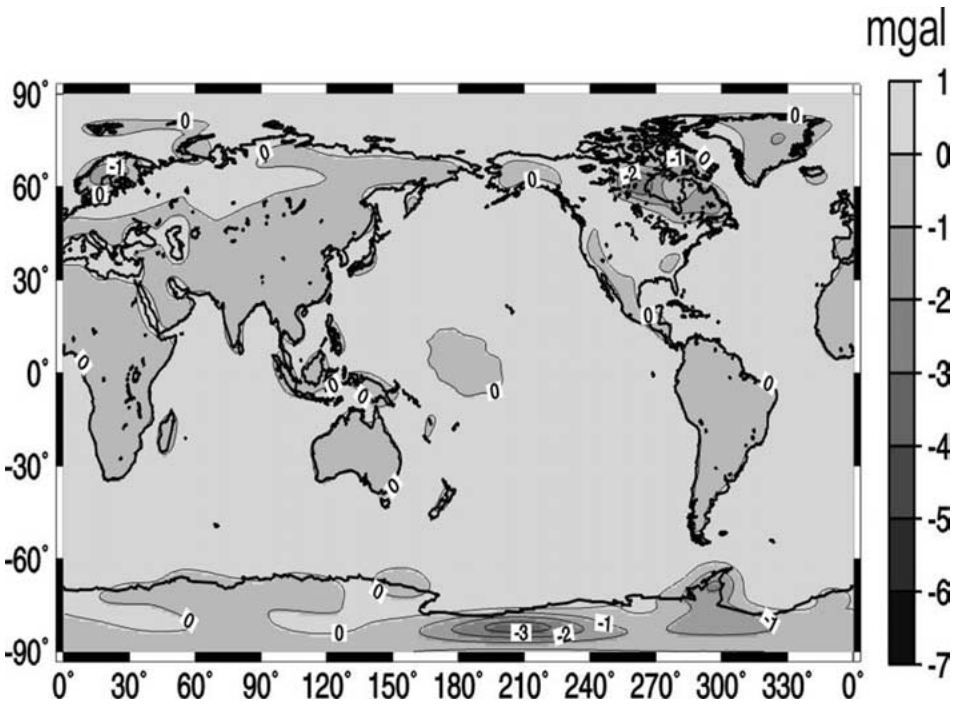

Figure 7. Global map of the modelled present day free air gravity anomaly (mGal) due to Pleistocene deglaciation, for spherical harmonic coefficients in the degree range l = 80–200. The contour interval is 1 mGal.

3.1.3. *Interpretation of Tectonic Processes and Motions*

The continental lithosphere is also exposed to tectonic processes, which in many places impact sea-level changes as much as, for example, GIA associated with PGR. Tectonic processes that result in vertical motion influence sea-level trends along the continental margins. Tectonic motions can be due to the active convergence between plates or to the density anomalies embedded in the upper mantle. For example, in the central Mediterranean region, the modelling of the tectonic motions (Di Donato et al., 2000) has shown that active convergence between the African and Eurasian plates and deep seated density anomalies are responsible for a sea-level signal superimposed on the eustatic and isostatic signals due to Pleistocene deglaciation. In the far field with respect to deglaciated areas, such as in the Mediterranean sea, the combined effects of density anomalies embedded in the lithosphere and plate convergence induce a sea-level signal which is comparable in magnitude with that due to the GIA. In the following, we detail those findings demonstrating by means of forward modelling that density anomalies in the upper mantle, which are in principle recoverable by GOCE due to their magnitude and spatial wavelength, are responsible for relative sea-level signals comparable with the characteristic error bounds in long term relative sea-level data. These findings indicate the major role of GOCE for a correct interpretation of the secular

component of sea-level data inferred from tide gauges, and from geological and archaeological data. This component influences the interpretation of present day trends in the variability of the Earth's climate.

In Figure 8 we portray the rates of vertical deformation in millimetres per year, based on a sensitivity analysis carried out in that part of the Mediterranean basin explored by Di Donato et al. (1999), where the density contrast between the Adriatic plate subducted underneath the Italian peninsula and the surrounding mantle is varied from 0 (in panel a) to 40 kg/m^3 (in panel b). These results can be directly interpreted as relative sea-level rates if the sign of these vertical rates is changed. The Adriatic plate is being thrust beneath the Italian peninsula from East to West, and the thick line, running almost parallel to the Adriatic coast of Italy, denotes the surface boundary of the Adriatic plate. The subducted portion of the Adriatic plate, where the density is varied, reaches a depth of 200 km.

These results include the effect of convergence between the African and Eurasian plates, in agreement with the model first implemented by Negredo et al. (1999). The changes in the rates of vertical deformation from (a) to (b) are thus due solely to the variation in the density contrast between the subducted Adriatic plate and the mantle. It is noteworthy that the coastlines of Italy are subject to subsidence, or sea-level rise due to active tectonics and deep seated density anomalies. If we focus on the eastern Adriatic coast of the peninsula, where sea-level records are available based on archaeological Roman ruins, we notice that changes in the density contrasts by 40 kg/m^3 are responsible for the migration of the -0.4 mm/yr isoline from inland in the northern basin, where Venice and Ravenna are located, to the coast, thus causing a variation of sea-level rise in the same locations along the coast of $+0.2$ mm/yr, corresponding to the error bounds in sea-level data obtained from archaeological inferences (Di Donato et al., 1999). These findings demonstrate that density changes in the lithosphere recoverable by GOCE should have an impact on the interpretation of relative sea-level data, because they induce a signal which is visible in sea-level records (Tscherning et al., 1999). This sea-level signal due to crustal density anomalies must be separated from the signal due to compactness of the sediments, which may not be a trivial task.

Figure 9 portrays the *gravity anomaly* in mGal along a profile perpendicular to the subduction zone across the central region of the Italian peninsula and Adriatic Sea, for a density contrast between the subducted slab and the surrounding upper mantle of 40 kg/m^3 as used in the sensitivity analysis. The *gravity* anomaly is positive because we are dealing with an excess of mass, and the amplitude of the anomaly of 3.5 mGal is comparable with the anomaly that will be recovered by GOCE. We can also note that the characteristic wavelength of the *gravity anomaly* responsible for the signal visible in the sea-level records is about 150 km, which is comparable to the spatial resolution of GOCE.

A comparison between tectonic and GIA results shows that the anomalous density structures at the lithospheric and upper-mantle level are responsible for the appearance of short-wavelength features in sea-level changes which are of

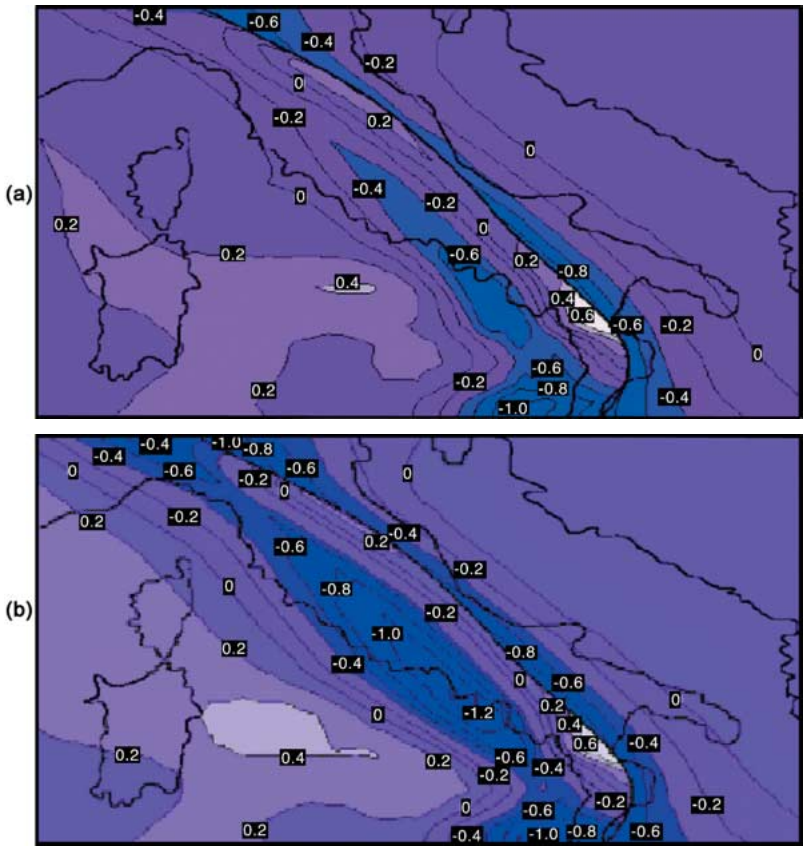

Figure 8. Rates of vertical deformation of the Earth's crust in the central Mediterranean, in particular in the Adriatic Sea and Italian peninsula, in the same area as explored by Di Donato et al. (1999). The modelled vertical deformation rates in millimetres per year are obtained from the three-dimensional finite element model first used by Negredo et al. (1999), which includes the active convergence between the African and Eurasian plates occurring at a relative velocity of 1 cm/yr. The finite element model takes into account the lateral variations in the lithospheric thickness in the area, and in particular the subducted lithosphere in the Calabrian Arc and in the Adriatic Sea. The mantle is described by a viscoelastic rheology with a viscosity of 10^{21} Pa s. In the upper panel (a) there is no density contrast between the Adriatic subducted lithosphere and the surrounding mantle, while in lower panel (b) the density contrast is fixed at 40 kg/m^3.

importance for a correct interpretation of sea-level data. A detailed knowledge of the density structure from GOCE will thus allow the risk of sea-level change in coastal areas to be better assessed. It will also allow the sea-level changes due to climate changes and anthropogenic activities to be quantified using the residual between the observed data and the modelled effects of tectonics and GIA. These conclusions, obtained for a specific region, can easily be generalised to the other areas where the lithosphere and upper mantle are varying laterally in their density structure due to active tectonics.

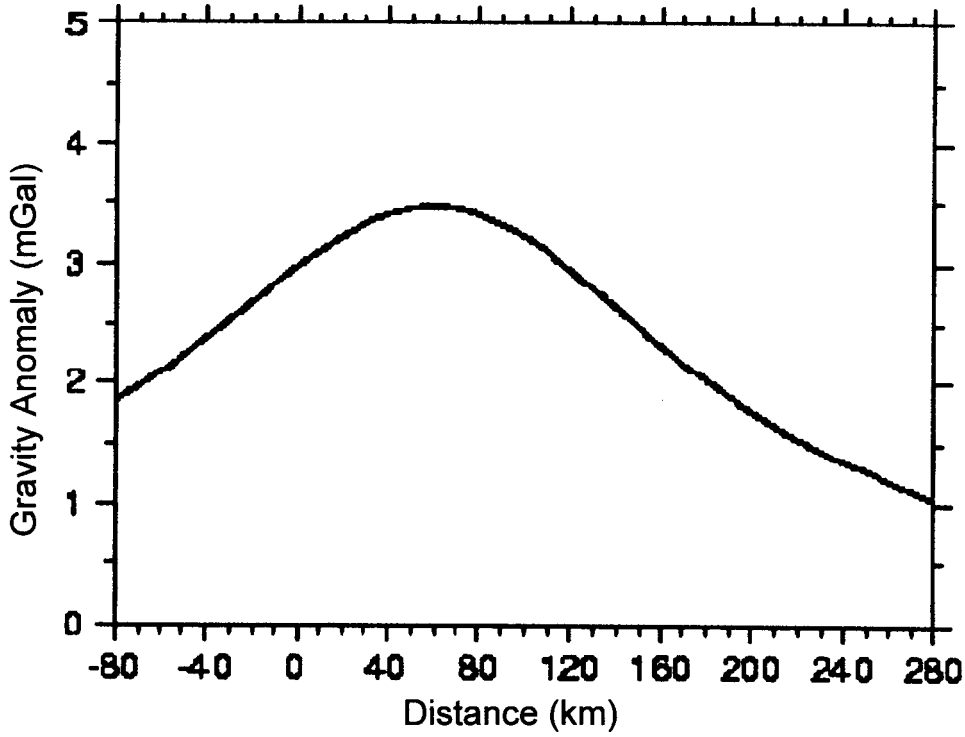

Figure 9. Gravity anomaly in mGal associated with a density anomaly of 40 kg/m^3 in the subducted Adriatic lithosphere along a North East oriented profile separating the western and eastern parts of the Italian peninsula across Tuscany.

3.2. OCEANOGRAPHY

While variations in the sea surface height and thus in the ocean currents can be derived directly from satellite altimeter data, an assessment of the absolute value of the ocean dynamic topography (and hence the absolute surface circulation) requires that the elevation of a hypothetical ocean at rest, i.e., the *geoid*, be subtracted from the altimetric mean sea surface height. The typical elevation scale of the dynamic topography is of the order of 0.1 to 1 m. The precision of present *geoid* models is similar on the scale of many ocean-circulation features. The calculation of the mean dynamic topography using mean sea surface height and *geoid* information can therefore not be satisfactory performed for degree larger than about 20 (or half-wavelengths less than about 1000 km) as, at that spatial-scale, the *geoid* model error becomes larger than the dynamic topography signals. The application of imprecise *geoid* models to the determination of dynamic topography at shorter spatial-scales can consequently result in the computation of false topographic signals < 1m which, in turn, correspond to erroneous transport calculations of several Sv (where 1 Sv = 10^6 m^3/s). Transport uncertainties of this magnitude are of significance in climate studies (Wunsch and Stammer, 1998).

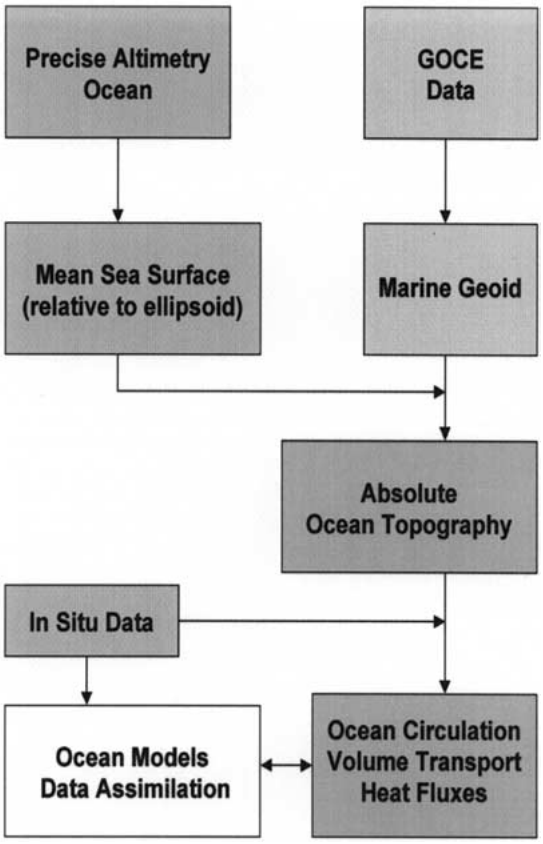

Figure 10. Diagram showing the improvement in absolute ocean circulation studies expected from a combination of the GOCE-produced marine geoid with precision altimetry.

The accurate and high-resolution marine *geoid*, as derived from GOCE, will in combination with precise satellite altimetry enable new estimates to be made of the absolute ocean topography (Figure 10). In combination with *in-situ* data and ocean models, this will, in turn, provide a high-resolution "window" on the ocean circulation at depth. Such improvements in estimates of the mean ocean circulation are much needed.

First, it is through mean flows, as well as variability (e.g., eddies), that the ocean transports its heat, fresh water and dissolved species. Both modelled and real oceans exhibit short-spatial-scale components of mean flows. It is important to be able to measure the locations and magnitudes of such short-scale features by means of altimetry and *gravity*, to compare them with the information obtained from conventional hydrography, to understand their relationships to bathymetry and other controlling factors, and to assess their importance for oceanic-mass and heat-flux estimations.

Secondly, because ocean eddies and other instabilities are generated by the mean flows, their levels of variability in numerical models depend much on the strength and position of the mean flows and on the parameterisation of the associated physical processes (e.g., interactions with bathymetry). Conversely, the variability can act as a brake on – or stimulant to – the mean flows by means of internal stresses. Consequently, in dealing with non-linear processes and in studying transient perturbations of the system, it is essential to understand both the variability of the ocean circulations and their transport of heat and mass.

Thirdly, data assimilation schemes for "ocean forecasting" have reached a stage of development where the optimal use of altimetric variability information can be achieved so long as the mean ocean state (i.e., the absolute ocean circulation) can be properly constrained. The dynamic topography, obtained from mean sea surface height minus *geoid*, will provide such a constraint on the mean surface circulation and will therefore also be beneficial to the assimilation of altimeter variability information as demonstrated by Le Provost et al. (1999).

3.2.1. *Interpretation of Circulation at Short-Spatial-Scales*

The mesoscale energy in the ocean topography (height) fields is centred on the 100–250 km half-wavelength band. The proper understanding of these short-spatial-scale dynamical processes is as important to the study of ocean circulation and its heat and mass transport as measurements at the largest (gyre, basin) scales, which are just about possible today.

The partitioning of the total ocean topography obtained using the 1/12° resolution MICOM ocean model of the North Atlantic (Paiva et al., 1999; Chassignet and Garraffo, 2001; Le Provost, 1999) into topographies corresponding to different spatial scales are shown in Figure 11; year 14 of the simulation has been chosen. While Figure 11a indicates the complete topography over all spatial-scales, Figure 11b shows the topography for scales with half-wavelength larger than 1000 km, and Figure 11c, d, e the parts of the topography with spatial-scales shorter than 1000, 250 and 100 km half-wavelength, respectively (i.e., approximately degree 20, 80 and 200, respectively).

Figure 11b can be seen to correspond essentially to the present situation in which *geoid* model uncertainties result in the mean sea surface (MSS) being separable from the *geoid* surface to approximately degree 20 only. Figure 11c simulates that part of the topography which is unresolved with present data sets, and which will remain unresolved without a *gravity* mission. Figure 11d indicates schematically that part of the topography such as the fronts associated with the Azores Current and western boundary currents which will remain unresolved even after a medium-resolution *gravity* mission (i.e., GRACE) is flown.

Figure 11e indicates that part of the dynamic ocean topography at the shortest scales which will remain unresolved to satisfactory precision after GOCE; it can be seen that most of the features in Figure 11d no longer remain in Figure 11e, with

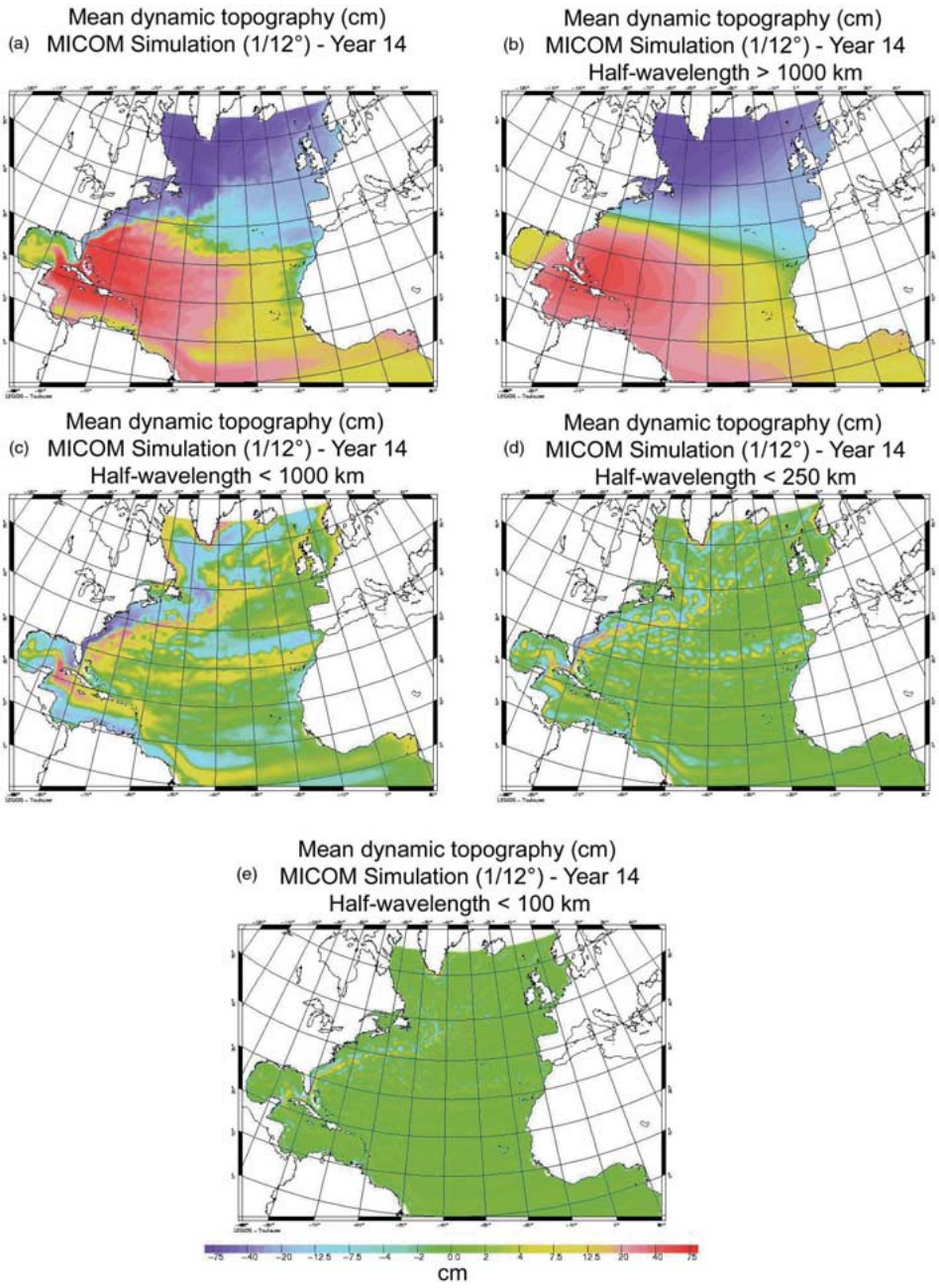

Figure 11. (a) Ocean topography over all spatial-scales obtained using the 1/12 degree resolution MICOM ocean model of the North Atlantic; (b) the same topography, but for scales with half-wavelength larger than 1000 km; (c, d, e) the same topography, but for spatial-scales shorter than 1000, 250 and 100 km half-wavelength, respectively.

the exception of small residual signals confined to coastal areas and sharp frontal zones.

Figures 12a, b, c present the corresponding *geostrophic surface currents* derived from the high-pass-filtered topographies of Figures 11c, d, e corresponding to half-wavelengths of 1000, 250 and 100 km respectively. These figures confirm the information provided by the topography maps. The 100 km half-wavelength cut-off implied by the relatively few remaining signals of interest in Figure 11e and Figure 12c is consistent with requirements for improved high resolution *geoid* models.

Knowledge of the eddy statistics of the real ocean from altimetry, together with a knowledge of the precise positions of the ocean jets from altimetry plus *gravity* (rather than from the assumption of frontal positions by means of sea surface temperature or hydrographic information, at present), will enable a more precise determination of the role played by the eddies in maintaining the jet components of the circulation to be made. For example, Hughes and Ash (2001) demonstrated that the interpretation of eddy-mean flow interactions in the Southern Ocean depends crucially on accurately identifying the location of narrow (100–200 km) fronts in the mean flow. *In-situ* hydrographic data are inadequate for the task of revealing these scales; sea surface temperature values derived from satellites can be a qualitative way to locate the fronts (Figure 13). While such data have sufficient resolution under cloud free conditions, and demonstrate clearly the small length scales of these features, they are not open to a quantitative interpretation in terms of ocean currents, and may be subject to unknown biases resulting from processes in the ocean surface layers. In order to take such analyses beyond qualitative comparisons, true mean *geostrophic surface currents* are needed at these frontal length scales. This is precisely what will be provided by GOCE in combination with altimetry, as the fronts are expected to have decimetric signals in sea-level relative to the *geoid*. Such analyses will, in turn, yield more reliable constraints and enable greater confidence to be placed in the construction of the next generation of ocean and climate models.

3.2.2. *Interpretation of Oceanic Flux Estimates*

Developments for merging the *gravity* information, which will be obtained by GOCE and other *gravity* missions, into ocean models have recently been discussed by Ganachaud et al. (1997), Wunsch and Stammer (1998), Woodworth et al. (1998), Le Grand and Minster (1999), Le Grand (2001) and Schröter et al. (2002). Figure 14 shows the dynamic topography of the South Atlantic Ocean obtained from classical hydrographic data. It indicates, in particular, the subtropical gyre in the North and the many fronts associated with the Antarctic Circumpolar Current (ACC) in the South. Superimposed on the map are a number of sections through which the potential improvements in volume flux estimates have been studied using a 1° inverse ocean model (Le Grand, 2001). An altimeter-derived MSS (with uncertainty set to 2 cm as an estimate of the precision of altimetric measurements at

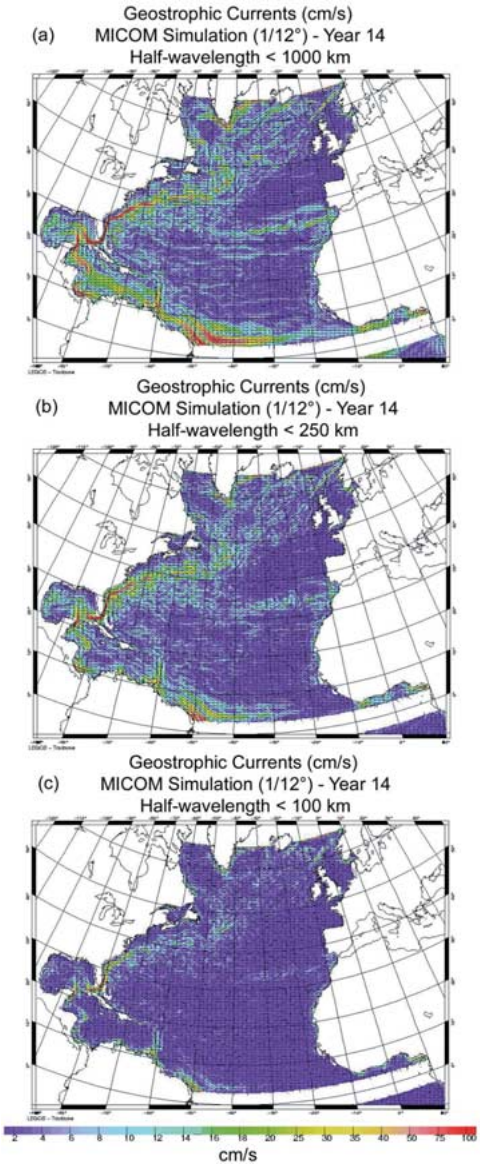

Figure 12. Intensity (see colour scale) of the geostrophic surface currents corresponding to spatial-scales of the topography with half-wavelengths less than 1000 (a), 250 (b) and 100 km (c), respectively.

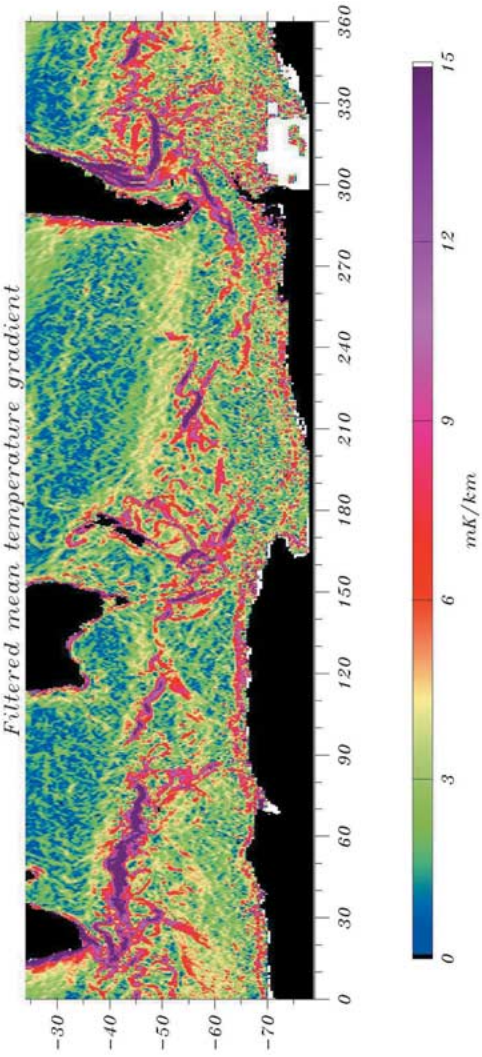

Figure 13. Filtered mean-sea-surface-temperature gradients in the Southern Ocean obtained from ESA's ERS/ATSR (Along Track Scanning Radiometer) indicating the presence of many short-spatial-scale features (Hughes and Ash, 2001).

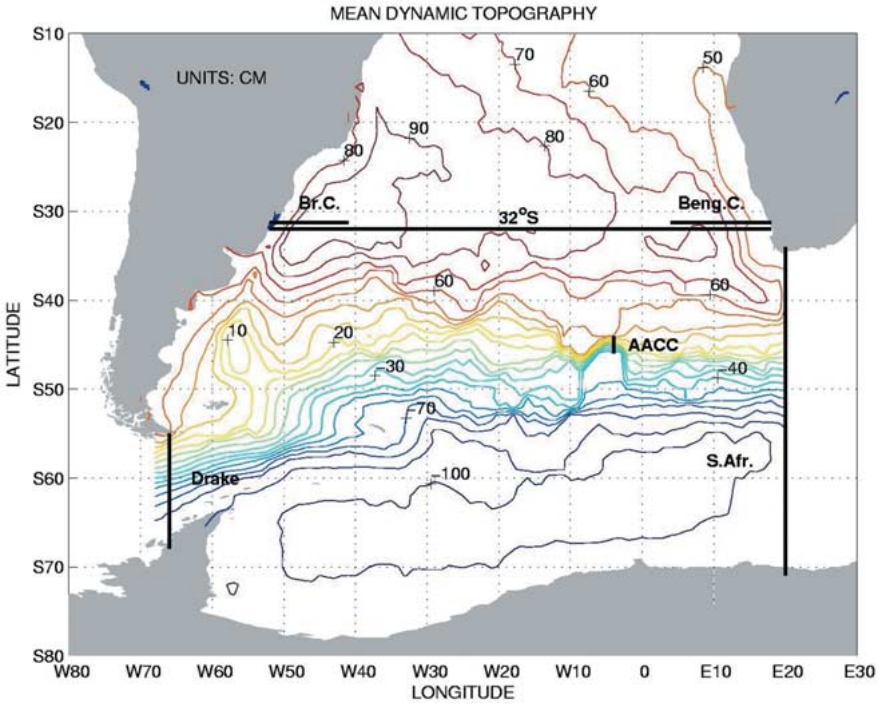

Figure 14. Mean dynamic topography of the South Atlantic Ocean determined from hydrographic data, upon which sections discussed in the text are superimposed. The contour interval is 10 cm ranging from the −100 cm (dark blue) in the Weddell Sea to +90 cm (brown) off the coast of Brazil.

the time of GOCE), hydrographic data, and either the current EGM-96 or potential GOCE *geoid* error fields (see Section 4) up to degree and order 180 were employed in the study.

Sections across the South Atlantic have been chosen to represent flows through the Drake Passage, a zonal section at 32° S between Africa and South America through the widest part of the sub-tropical gyre, a short section through a sharp front in the Atlantic sector of the Antarctic Circumpolar Current (ACC) close to the Greenwich meridian (labelled AACC), the South African ACC "choke point", a section across the Brazil Current (Br. C.) and a section across the Benguela Current (Beng. C.). Figure 15 indicates the reduction in uncertainty of transports through each of the sections when using the anticipated GOCE error spectrum compared with that currently available from EGM-96. For each section, the reductions for the entire water column, for surface waters and at depth, are shown. The transports estimated in the reference EGM-96 calculation and the associated uncertainties are indicated in parentheses.

The layers considered in this study have been chosen to represent the various dynamical regimes present in the ocean. For example, transports in the entire water column correspond to inter-basin exchanges of volume. Transports in the upper 100

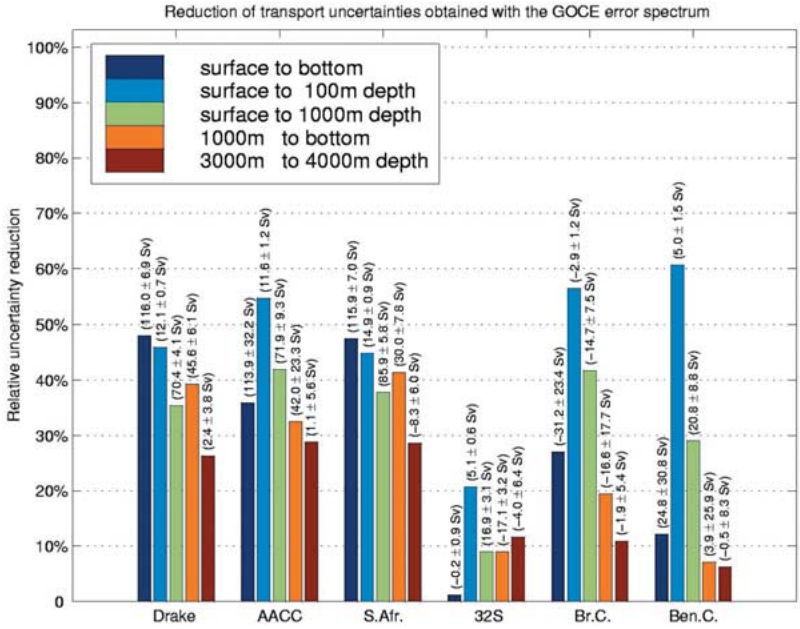

Figure 15. Reductions in uncertainty of volume transports within an inverse ocean model when simulated GOCE errors are employed instead of those of EGM-96 for the Drake Passage, the short section across the ACC near to the Greenwich Meridian (AACC), the South African 'choke point', the 32° S African-South American gyre section, the Brazil Current section and the Benguela Current section. Numbers in parentheses show the transports (in Sv) obtained by the model using the present-day EGM-96 model, together with their uncertainties.

m of the water column roughly correspond to the layer where Ekman transports (direct wind-driven surface flows) take place. The uncertainties in these Ekman transports are larger than the uncertainties in the geostrophic transports (of the order of 1 Sv) obtained with the current EGM-96 error budget and limit the impact of the determination of the latter. However, the Ekman transport uncertainties can be expected to be greatly reduced in the future, as more precise wind scatterometer observations become available. Finally, the transports in the upper kilometre of the water column correspond to the upper branch of the *meridional overturning*, while transports below 1 km depth correspond to the lower branch of this circulation. The present estimate of the uncertainties in these transports is approximately 10%. This uncertainty level should not give the false impression that the *meridional overturning* and its transport are already known sufficiently. Indeed, the remaining uncertainties are still large in terms of our knowledge of the climate system and, perhaps more importantly, in terms of the detection of potential climate changes. A climate change of the order of the present-day uncertainties is likely to have a large effect on the environment because the transports of heat associated with the *meridional overturning* are huge (typically 1 Sv of volume transport corresponds to a heat transport of 5×10^{13} W at mid latitudes, of the order of 5% of the total

heat transport in a single ocean basin). As such, the reduction of these uncertainties by means of data from a *gravity* mission is of great importance.

The largest reduction in transport uncertainty occurs in the upper ocean, which is not surprising because reduced *geoid* errors will directly provide precise constraints on upper ocean velocities. The overall reductions are very significant, being over 50% for the top 100 m of the short ACC section and up to 40% for the top kilometre. In the deep-ocean, the relative impact of GOCE is also significant, with a reduction of 30% in the uncertainty in the ACC transport. Such reductions follow from the major improvements in *geoid* model accuracy to be expected for remote areas of the ocean and will be of major importance to climate modelling. The impact on surface-to-bottom transports is also large for the three sections located in the ACC, reflecting its barotropic character.

The impact on uncertainties in transports across the South Atlantic gyre at 32° S is smaller than the impact in the other sections. The impact on uncertainties in surface-to-bottom transports is negligible because the total transport is constrained by mass conservation to be zero within small error bars, and cannot be further reduced. The impact on surface transports is larger, but it is still much smaller than the corresponding impact found in the ACC sections. On the other hand, the impact on the shorter sections at 32° S across the Brazil Current and the Benguela Current is much larger. The reduction of transport uncertainty reaches 60% in the upper 100 m and 40% in the upper kilometre, which is similar to the impact found in the ACC. This result suggests that the impact of *gravity* missions cannot be measured by looking at trans-oceanic sections only, especially in the case of a high-resolution mission like GOCE. Similar conclusions were recently obtained for the estimates of transport through the Florida Strait made by Schröter et al. (2002).

In summary, the impact of GOCE will be significant for transport estimates in the upper ocean. The largest absolute impact (about 10 Sv) is associated with the short section in the ACC while the largest relative impact is associated with the sections across intense oceanic jets like the Brazil Current and the Benguela Current. This is consistent with the expectation that the GOCE mission will have a larger impact on narrow and intense currents. Many of these transports, which constitute the upper branch of the *meridional overturning*, play an important role in the redistribution of heat from the equator to the poles. As such GOCE will contribute to improvements of our understanding of the global climate system.

3.3. GEODESY

Geodesy is concerned with the measurement of the Earth's shape. Whereas positioning on the Earth's surface in two- or three-dimensional co-ordinates is based on purely geometric techniques, height determination requires a knowledge of the Earth's *gravity* field. Only through a knowledge of differences in *gravity potential* is it possible to decide on the direction of the flow of water. The traditional, very cumbersome and slow, technique of height determination is by means of geodetic

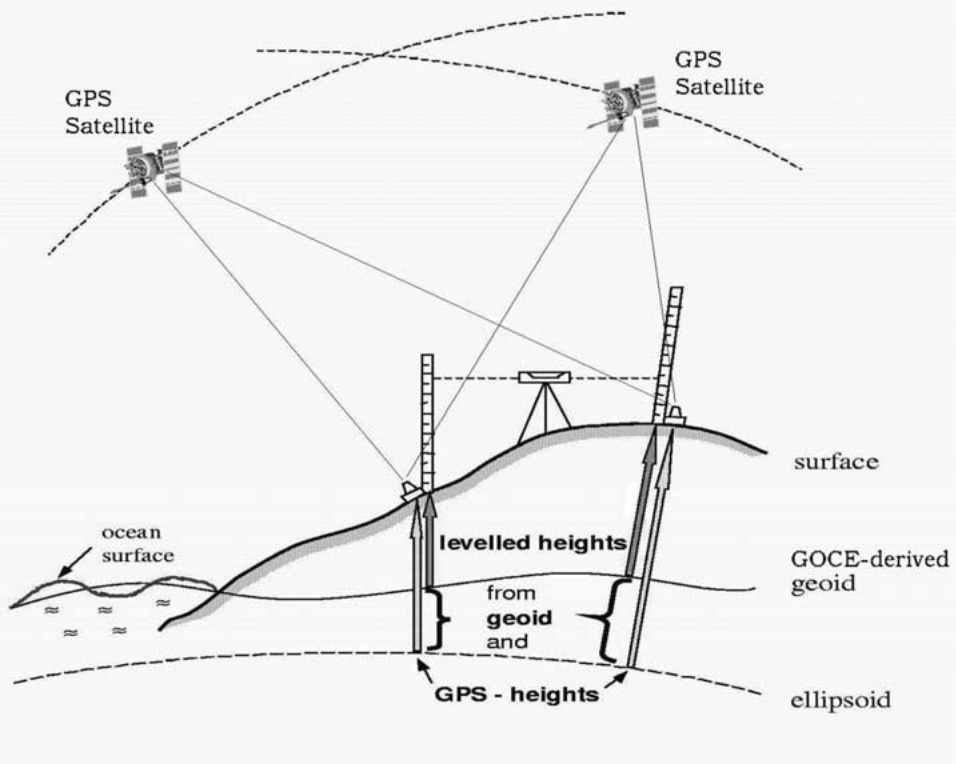

Figure 16. Diagram showing the concept of levelling by GPS. Differential GPS provides ellipsoidal heights at terrain points (GPS heights); with precise geoid heights about the same adopted reference ellipsoid, GPS heights can be converted to orthometric heights (levelled heights).

levelling in combination with gravimetry. Geodetic levelling attains mm-precision over smaller distances, but is subject to systematic distortions on continental scales.

A global *geoid* of 1 cm accuracy at about 100 km spatial resolution and a *gravity* field model with 1–2 mGal precision accuracy and the same spatial resolution would serve five major objectives in geodesy. These are addressed below.

3.3.1. *Levelling by GPS*

In a similar way as ocean altimetry combined with the *geoid* determines dynamic ocean topography, the combination of GPS and *geoid* determines land topography and topographic heights (Schwarz and Sideris, 1987; Rummel, 1992). In other words, with the aid of *geoid heights* above an adopted *mean Earth ellipsoid*, geometric heights above this ellipsoid, as determined by GPS or any follow-on system, are convertible to topographic heights relative to the *height datum* (generally parallel to the geoid). The latter are denoted as *orthometric heights* (see Glossary). The principle of this conversion is illustrated in Figure 16.

3.3.2. *Unification of Height Systems*

There are still a large number of unconnected height systems in use around the world. Each system refers to a reference point, usually a benchmark close to the sea and connected by levelling to mean sea-level obtained by a tide gauge. The discontinuity in height systems is of no importance as long as there is no requirement to compare height values from the various systems. In the past, discontinuities had to be accepted whenever different geographical areas (with their own individual height systems) were separated by sea (and/or borders between countries).

With the *geoid* precision to be achieved by GOCE, it will be possible to connect all height systems with cm-precision, provided that at least one benchmark in each height system is equipped with precision space positioning such as GPS (see, e.g., Heck and Rummel, 1990; Xu and Rummel, 1991: Khafid, 1998; Arabelos and Tscherning, 2001). Therefore, GOCE will, for example, bring all sea-level recordings into one height reference system, thus facilitating the reconstruction of longer sea-level records from presently disconnected nearby sites. In addition, it will eliminate height discontinuities between adjacent islands, and allow the removal of frequently encountered biases in terrestrial *gravity anomaly* data sets (i.e., height datum offsets, distortion in gravity networks, long wavelength errors).

3.3.3. *Improvement of Regional Gravity Field Knowledge*

There exist many regional sets of dense gravity measurements. They are used to determine the *geoid* locally, for tectonic studies and for geophysical prospecting, to a resolution corresponding to the density of the data. For each of these applications, use will be made of the very accurate models coming from GOCE, though limited to about 100 km half-wavelength. Furthermore, usage of surface gravity data at their full resolution requires that no bias or trend affect the data. Hence, the GOCE retrieved *gravity anomaly* (as derived from Equation (2.2.4)) will be used to correct for such errors by fitting the regional structure of the survey data to the GOCE field.

3.3.4. *Separation of Inertia and Gravity in Inertial Navigation*

The core sensors of any inertial measuring unit (IMU) for performing navigation are a set of gyroscopes and accelerometers. These two units are either mounted on a space-stable (or levelled) platform or rigidly fixed to the vehicle to be navigated. IMUs are employed in land vehicles, for aircraft or missile guidance, in submarine navigation, pipeline maintenance and bore-hole control. The principle is quite simple: the accelerometers measure vehicle acceleration, and single and double integration yield velocity and position differences, respectively. Changes in the orientation of the accelerometer triad are taken into account by the gyros.

However, one fundamental source of error is that the accelerometers measure not only vehicle motion, but the sum of vehicle and *gravity* acceleration. At present, the *gravity* part has been taken into account via a simple ellipsoidal *gravity* model. As a result, all deviations from an ellipsoidal *gravity* field are interpreted erroneously as vehicle accelerations. Precise knowledge of the *gravity* field, as

provided by GOCE, will serve to reduce this source of error significantly and either allow an increase in the time intervals between which velocity or positioning updates are required or simply improve overall accuracy (see Schwarz, 1981; Forsberg, 1985).

3.3.5. *Orbit Determination*

In addition to a further enhancement of past and future altimetric data sets for applications in oceanography and climatology as outlined above, a high-accuracy *gravity* field model will provide a significant improvement in orbit computations for Earth-orbiting satellites. It will lead to a better understanding of the physics behind orbit perturbations. Especially for low-orbiting satellites, it is foreseen that such a model will enable the separation of perturbations due to the static *gravity* field from those due to other perturbing forces. The latter include not only non-conservative forces caused by atmospheric drag and solar radiation, but also perturbations caused by the solid Earth and ocean tides.

This in turn will contribute to a further reduction of in orbit determination errors for Earth-orbiting satellites. Thus, for example, not only will the *gravity* field induced radial orbit error be reduced for altimetric satellites, but also the orbit error resulting from inaccuracies in modelling other perturbations, non-conservative forces in particular. The latter inaccuracies may be aliased into existing models; they are of the order of several centimetres for many altimetric satellites, such as GEOSAT, ERS-1 and -2, and Envisat. Improved re-analysis of the old altimetric data sets will be possible. In addition, orbits will be improved in the flight direction and in the direction perpendicular to the orbital plane. This will significantly simplify and facilitate the use of, for example, synthetic aperture radar (SAR) images taken by the ERS and Envisat satellites for many applications including interferometry. Finally, improvements in modelling orbit perturbations will lead to more accurate orbit predictions, enabling the near real-time operational use of not only altimeter observations for oceanographic applications but also satellites carrying a GPS or GPS receiver for atmospheric sounding as input for weather-prediction models.

3.4. GLOBAL SEA-LEVEL CHANGE

Global-averaged sea-levels are considered to have risen by between 10 and 25 cm during the past century, and are predicted to rise by the order of half a metre in the next century (Warrick et al., 1996). This will have important consequences for more than half of the World's population which lives within coastal zones, and which depends on the agricultural and industrial productivity of coastal regions, or which have to be protected from coastal flooding (Bijlsma et al., 1996).

It is essential that we attempt to understand the various components of sea-level change at the coast, rather than simply observe the combined effect of several mechanisms with networks of tide gauges, if accurate predictions are to become

possible (Church et al., 2001). In addition, it is clear from inspection of the historical tide-gauge data set, and from a study of currently available models, that future sea-level changes resulting from the various climate and geological processes will be anything but globally uniform.

GOCE can improve our understanding of past sea-level changes, and thereby improve predictions of future changes, in at least four ways (Visser et al., 2002):

- A high resolution and accurate *geoid* will result in more reliable determinations of ocean heat and volume fluxes that can be used to improve the General Circulation Models (GCMs) employed to model sea-level change due to thermal expansion (Bryan, 1996)
- More accurate models of GIA (e.g., Peltier, 1998) and of local tectonics will result in more precise estimates of the rates of "real" global- and regional-average sea-level changes during the past century by reanalysis of the historical tide-gauge records. This will provide tighter constraints within which to assess the quality of hindcast sea-level trends from climate models
- The improvements in reliability of "GPS minus *geoid* levelling" will ensure more feasible combinations of sets of short historical tide-gauge records (dispersed through a region) into regional composites
- The improvement of in orbit computation will lead to a reduction in geographically-correlated orbit errors in multi-decadal altimetric time series of sea-level anomalies; currently these are of the order of a few centimetres. This will, in turn, benefit studies of dynamic topography, low-frequency ocean circulation variability and long-term quasi-global sea-level change. It will also enable the direct use of altimeter data from any repeat, or non-repeat, orbital cycle by the provision of a common, precise reference surface.

4. Recovery of Gravity Field and Geoid

The GOCE mission concept has been conceived and designed to provide the most accurate, global and high-resolution map of the gravity field and its corresponding geoid surface, taking into account the research objectives discussed in the previous section jointly with advanced technological solutions. It will combine the satellite gradiometry (delivering medium to short wavelength observations) and the satellite-to-satellite high-low tracking (SST-hl, delivering long to medium wavelength observations) techniques that have been found to be optimum for providing the required high-quality, high-resolution static *gravity* field.

The quantitative requirements for the different multidisciplinary scientific goals are summarized and expressed in terms of *geoid height* and *gravity anomaly* accuracies in Table II, together with the corresponding spatial resolution to which they apply (expressed in half-wavelengths). The possibility to recover the *gravity anomalies* and *geoid height* to these accuracies is further highlighted in this section based on closed-loop and end-to-end simulations (Oberndorfer et al., 1999; Sünkel

TABLE II

The requirements (discussed in Sections 2 and 3) expressed in terms of geoid height and gravity anomaly accuracies (Orbits*: 1 cm radial orbit error for altimetric satellites)

Application	Accuracy		Spatial resolution
	Geoid (cm)	Gravity (mGal)	(have wavelength, D, in km)
Solid earth			
Lithosphere and upper-mantle density structure		1–2	100
Continental lithosphere:			
• Sedimentary basins	1–2	50–100	
• Rifts	1–2	20–100	
• Tectonic motions	1–2	100–500	
Seismic hazards	1	100	
Ocean lithosphere and interaction with asthenosphere	0.5–1	100–200	
Oceanography			
– Short	1–2		100
	0.2		200
– Basin scale	∼0.1		1000
Geodesy			
– Levelling by GPS	1		100–1000
– Unification of world-wide height systems	1		100–20,000
– Inertial navigation system		∼1–5	100–1000
– Orbits*		∼1–3	100–1000
Sea-level change	Many of the above applications, with their specific requirements, are relevant to studies of sea-level change.		

et al., 2000). These simulations, which include the *time-wise approach* (Balmino et al., 1999), reveal the precision of the spacecraft position recovered from SST, the precision of the gradients obtained from the gradiometer, and subsequently the accuracy of the *gravity* model that will be derived under the baseline mission and instrument characteristics (Touboul et al., 1999).

The analysis of the mission performance consists of two major stages and is supported by a mature, although complicated, overall procedure of data processing (CIGAR, 1996; Sünkel et al., 2000). First, the reliability and quality of the satellite measurement system is established. This is achieved by a comprehensive analysis and simulation of the gradiometer and SST-hl receiver characteristics themselves, and of their interaction with the satellite and the satellite environment. The raw data (Level 0) contain the readouts from the instruments, together with calibration,

time, attitude and orbit control system and drag-free control data, and other housekeeping information such as temperatures. The data are pre-processed (Level 1a) and used together with calibrated and corrected *gravity gradients*, linear accelerations, thruster activity parameters, and attitude, angular velocity and acceleration information (Level 1b data).

Secondly, this, together with a first estimate of the GOCE orbit, make it possible to refer the *gravity gradients* to an Earth-fixed reference frame. In so doing, use is moreover made of accurately defined reference systems and the precise ephemerides of the GPS satellites (as computed on a routine basis in the framework of the International GPS Service). Once processed, the Level 1a and Level 1b data will be further transformed and processed to the about 90000 global *gravity* field and *geoid* model parameters (Level 2). Then the stability of the computation and the propagation of the error characteristics from the data along the orbit at altitude to the *gravity* field parameters on the Earth's surface will be assessed. The Level 2 products will in turn be used as a starting point for scientific analyses (Level 3) as already addressed in Section 3.

The mission and instrument characteristics are summarized in Table III. As already mentioned, the reference GOCE orbit is a Sun-synchronous, circular, dawn-dusk low Earth orbit with an inclination of 96.5° at a design altitude of 250 km. The mission lifetime is 20 months for a total measurement duration of 12 months (3 months commissioning phase, 5 months hibernation due to eclipse). Using a drifting orbit (no exact repeat) a dense coverage with a pattern of inter-ground track distances not larger than 85 km at the equator can be obtained after 30 days. This may be made denser with time depending on the altitude window selected. The smallest recoverable wavelength (as shown by the simulation) requires a measurement sampling interval of 4 seconds. A one-second sampling time is recommended, which is not demanding on the overall system. Drag compensation, which is essential to enhance the mission capabilities, is assumed. Further information about the mission preparation, including status of the instrument development can be found at the web site http://www.esa.int/livingplanet/goce.

The fundamental observables that will be used for the reconstruction of the *gravity* field by means of the *gravity* gradiometry technique are the three diagonal components of the *gravity gradient* tensor expressed in Eötvös ($1E = 10^{-9}\,s^{-2}$). Their measurement errors, as affected by instrument errors, instrument-satellite coupling errors, satellite errors and post-flight on-ground processing errors, in the measurement bandwidth (frequency range) from 5 mHz to 100 mHz, are found to fall below 5 mE/ $Hz^{1/2}$. Both the gradiometer and the satellite performance have been optimised to minimize the errors of the *gravity gradients* (i.e., Equation (2.2.6)) in the measurement bandwidth.

The recovery of the *spherical harmonic coefficients, geoid* and *gravity anomaly* error spectra have been simulated using covariance propagation analysis (ESA, 1999). Stabilisation of the resulting system of linear equations has been achieved making use of error degree variances of a recent global model (satellite only solu-

TABLE III

Baseline mission and instrument characteristics. The errors in position are obtained by including the errors of real GPS phase measurements, of the propagation of dynamic model errors and of the IGS orbits (Visser and IJssel, 2000). The noise characteristics of the accelerometer take account of most recent instrumental studies and developments (Touboul et al., 1999) for spacecraft (attitude, self gravity) and system error sources (Aguirre-Martinez and Cesare, 1999). The orbit error values are r.m.s. values derived from a coloured error power spectral density

Measurement duration	12 months	
Orbit	almost circular, 250 km, 96.5° (Sun-synchronous)	
Position errors in monitoring the SST high-low	Δx (along-track)	2 cm/Hz$^{1/2}$
	Δy (cross-track)	1 cm/Hz$^{1/2}$
	Δz (radial)	3 cm/Hz$^{1/2}$
Gravity gradiometer error spectrum	Full diagonal instrument (V_{xx}, V_{yy}, V_{zz}) frequency $f < 10^{-3}$ Hz: f^{-1} coloured noise 5×10^{-3} Hz $< f < 10^{-1}$ Hz, white noise $< 5 \times 10^{-3}$ E/Hz$^{1/2}$	
Measurement sampling time	1 second	

tion) and signal degree variances of *Kaula's rule*. The maximum spherical degree and order that has been resolved is $L = 300$. This corresponds to a half-wavelength of $D = 65$ km. The results of these computations, i.e., the errors on the *gravity* field coefficients, the *geoid height* and the *gravity anomaly*, represent the expected scientific performance of the GOCE mission. Table IV contains an extract of these results, while the full triangular error spectrum of *spherical harmonic coefficients* is displayed in Figure 17.

In comparison with the specific measurement goals, the simulated r.m.s. errors of the recovered *geoid height* and *gravity anomalies* at the 100 km length scale reach values of about 0.25 cm and 0.1 mGal, respectively.

These results can also be visualized by mapping the retrieval errors as a function of colatitude (90° – latitude) by propagating the covariance error characteristics onto the sphere for the *geoid* and *gravity anomalies*. This is shown in Figure 18. The errors show some weak latitude dependency down to about 7° below which the errors increase by up to about one order of magnitude due to gaps in the two polar regions. Elsewhere, the level of the r.m.s. curves is consistent with the cumulative errors up to the specified maximum degree L.

The distortions in the spherical harmonic error spectrum caused by a non-polar orbit are of little concern because it is clear from Figure 18 that these distortions are perfectly mapped back to the polar regions. A strict lack of data over the pole would therefore not degrade the use of the GOCE results for the main applications. On the other hand, this situation may be improved by including the results from

TABLE IV

Expected r.m.s. errors in the geoid height and gravity anomalies at given resolutions, as derived from the GOCE baseline mission simulations. At resolutions where the regularisation of the inverse problem plays a role (i.e., at scales finer than 100 km) the numbers are approximate

Spatial resolution (half-wavelength)	Maximum degree L (corresponding to D)	Geoid height (mm)	Gravity anomaly (mGal)
1000 km	20	0.4	0.0006
400 km	50	0.5	0.001
200 km	100	0.6	0.03
100 km	200	2.5	0.08
65 km	300	∼45	∼2

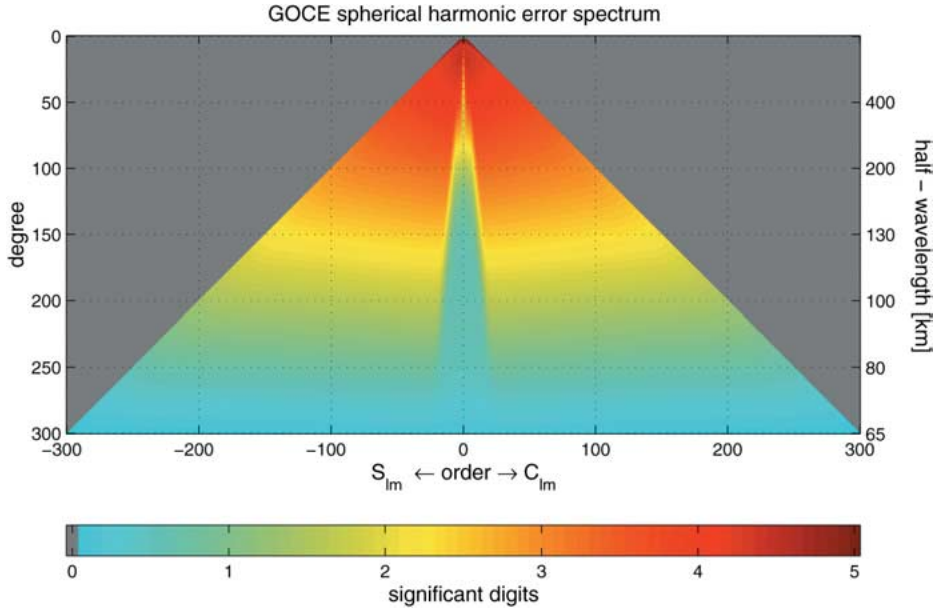

Figure 17. GOCE spherical harmonic error spectrum. The vertical axis of the triangle refers to the spherical harmonic degree l (or to the corresponding spatial resolution D), the horizontal axis to the order m of the coefficients, with the C_{lm} coefficients on the right and the S_{lm} coefficients on the left. Thus the coefficient C_{00} would be located at the top of the triangle, whereas the coefficients with increasing degree and order refer to smaller and smaller scales of the gravity field. The colour code refers to the number of decimal digits (significant digits) to which the individual coefficients can be resolved. For example, two significant digits mean a determination of coefficients with only 1% uncertainty.

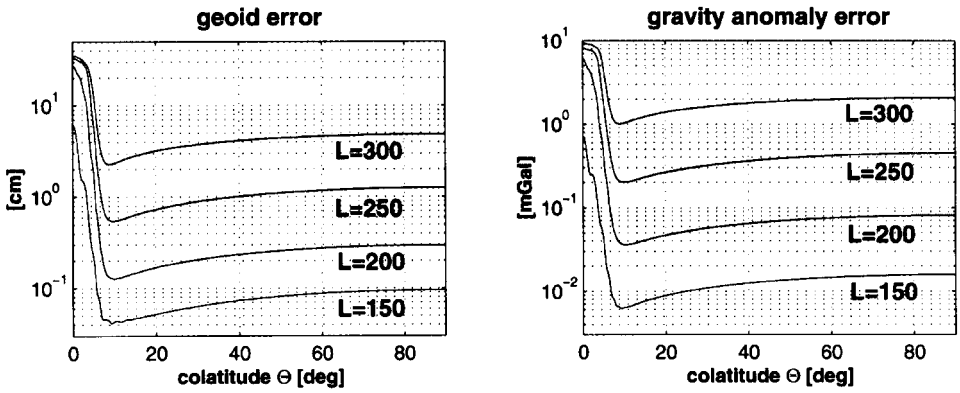

Figure 18. Accumulated point error on the geoid [left] and gravity anomaly [right], for series expansions up to degree and order $L = 150$ ($D = 135$ km), $L = 200$ ($D = 100$ km), $L = 250$ ($D = 80$ km), $L = 300$ ($D = 65$ km), as a function of colatitude for the northern hemisphere (the results are symmetrical with respect to the equator), from the GOCE baseline mission simulation. The errors decrease when going towards the pole due to the accumulation of satellite ground tracks, and then increase due to the polar gap.

more aero-gravimetric campaigns over the Arctic and Antarctic; these have been carried out in the Arctic region and are planned for the Antarctic area in the years to come, and will help to close the two gaps. In any event, the *gravity anomaly* error at, for instance, 100 km length scale (curve with maximum degree $L = 200$ in Figure 18) remains below 7 mGal close to the poles and below 1 mGal about 5° of colatitude away, which is quite an astonishing and useful result over those remote areas.

Finally, it should be emphasized that the gradiometer is three-dimensional, i.e., it simultaneously measures the gravitational field in all three spatial directions. Consequently the errors of the resulting *gravity* parameters (*gravity anomalies* or *geoid heights*) exhibit no preferred direction. Apart from the redundancy, the errors are independent and isotropic. This isotropy of the error structure is of great advantage, in particular when the directional structure of the gravitational field is of importance, as is the case in oceanography where slopes of dynamic topography are to be derived.

The results of the performance simulation consequently confirm that the GOCE baseline mission will be unique. The recovery of the best possible set of spherical harmonic coefficients of the Earth's *gravity* field and precision orbit will ensure that the derived products (i.e., *geoid height* model, *gravity anomaly* model, and *gravity gradients*) will clearly fulfil the observation requirements in solid Earth physics, oceanography and geodesy as listed in Table II and quantified by the impact analyses in Section 3.

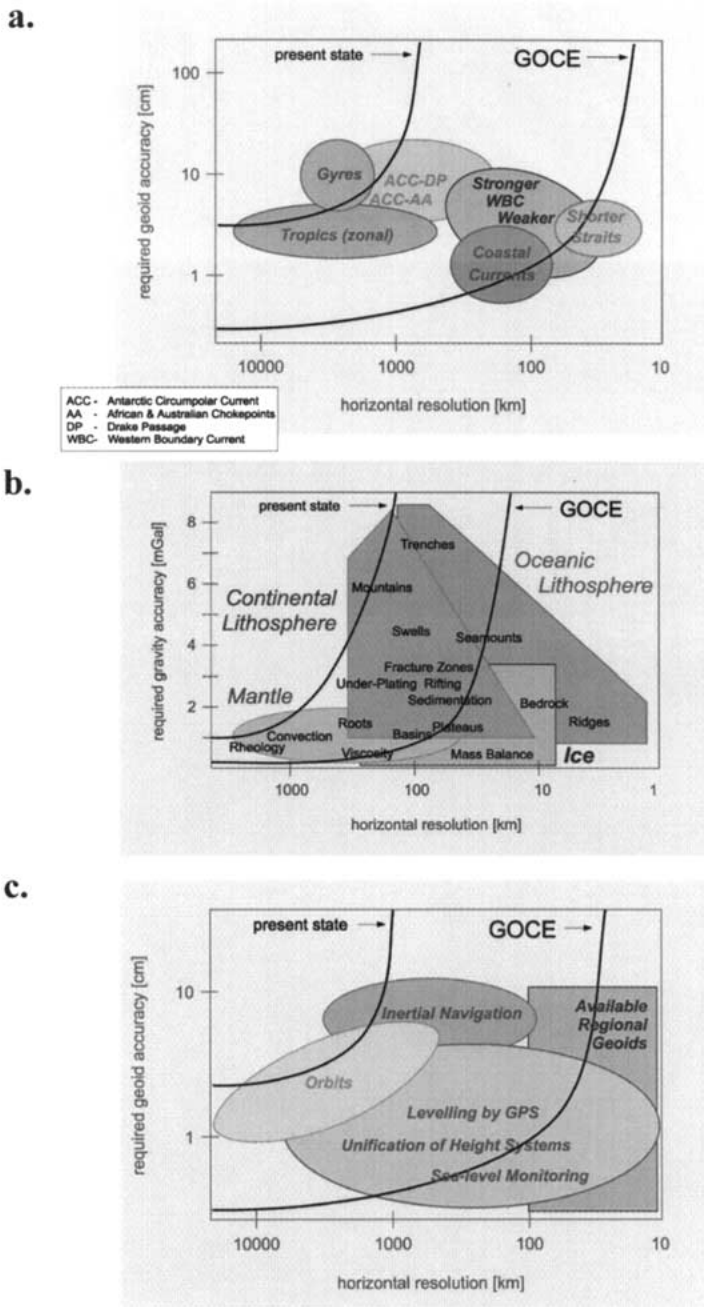

Figure 19. Simulated GOCE retrieval accuracy compared with present knowledge mapped in a diagram of the required accuracy (estimated at approximately 10% of the corresponding signal strength) as a function of spatial scales for a variety of features, process and phenomena occurring in (a) oceanography, (b) solid Earth physics and (c) geodesy.

5. Summary

The GOCE mission, planned for launch in 2006, will combine satellite gradiometry and SST-hl to produce a new model of the *gravity* field of unprecedented accuracy and spatial resolution. Its main products will consist of sets of *spherical harmonic coefficients* up to a maximum degree and order 300, which will describe the global *gravity* field and *geoid*. In addition, a range of detailed global and regional *gravity anomaly, gravity gradients, geoid* and *geoid* slope maps or gridded data sets will become available to the scientific community. All of these primary products will be accompanied by estimates of their error standard deviations and correlations. Although these products will clearly become available only after the mission, it is already anticipated that the real error estimates will be very similar to those obtained from the full simulation of the system performance from sensor level to the retrievals of the *gravity* field and *geoid* signals. For instance, up to degree 200 (100 km resolution half-wavelength) GOCE yields a *geoid* error at the 2.5 mm level, and a *gravity anomaly* error just below 0.08 mGal, for the static field. Using these simulated error estimates, it has been possible to assess reliably the impact which GOCE is expected to make in the fields of science and applications as discussed in this paper in the context of solid Earth physics, oceanography and geodesy, and schematically summarized in Figure 19.

Solid Earth. In solid Earth physics the production of the GOCE *gravity* model is not in itself the primary goal; rather it is the provision of a detailed three-dimensional image of density variations in the lithosphere and upper mantle, derived from a combination of *gravity*, seismic tomography, lithospheric magnetic anomaly information and topographic models. This density image is well constrained by knowledge of the *gravity* field. The density information then allows precise quantitative modelling of sedimentary basins, rifts, tectonic motions and sea/land vertical changes.

Absolute Ocean Circulation. With the mean dynamic ocean topography derived from the GOCE *geoid* in combination with precise altimetry and *in-situ* observations (i.e., such as by the planned deployment of the array of up to 3000 *Argo* profiling floats (see http://www.argo.ucsd.edu and http://www.coriolis.eu.org) by 2004 (Roemmich and Owens, 2000), practically all ocean current systems from the strongest (Gulf Stream, Kuroshio, Antarctic Circumpolar Current) through to weaker deep-ocean and coastal current systems should be determined in terms of location and amplitude. The high-spatial-resolution *geoid* afforded by GOCE has been demonstrated to reduce the uncertainties in mass and heat transport by a factor of 2 in the upper layers, with significant reductions throughout the water column. Clear benefits are also expected in high-resolution ocean forecasting (Le Provost et al., 1999).

Geodesy. GOCE data will serve four major challenges in geodesy. It will, in combination with GPS, help to produce a worldwide unification of height systems. Moreover, it will have a practical impact in reducing the source of error for inertial navigation, and it will lead to significant improvement in orbit computations for Earth-orbiting satellites.

Finally, there are fields of application where the benefits of GOCE enter via several directions. For example, the study of sea-level changes spans research into changes in ocean circulation, steric changes (expansion and/or contraction of a body of sea water induced by variation in temperature and salinity) and changes in ocean volume, vertical land movements, ice mass changes, height systems and satellite orbits. GOCE data will facilitate more comprehensive investigation of complex topics including, for example, a comparison of sea-level and sea-level changes in the North Sea with those in the Mediterranean.

In addition to complementing classical altimetric missions, the scientific results from GOCE will be perfectly complemented with observations from other gravity missions such as CHAMP and GRACE, and from new dedicated missions to observe the cryosphere such as ICESat (2002) and CryoSat (2004). In particular, the different technical concept of GRACE, launched in March 2002, will recover the gravity field with very high precision for the long and medium spatial scales and thus support GOCE data processing for the recovery of the accurate short scale gravity anomalies. For instance, Wahr et al. (2002) suggest that methods could be developed to infer changes in deep ocean currents from GRACE measurements of time-varying gravity at temporal and spatial scales of around 30 days and 500 km. In conclusion, we are convinced that the expected increasing availability of data from these dedicated gravity field missions within the next 5 years will introduce a new era for multi-disciplinary research and application in solid Earth physics, oceanography and geodesy. (The website http://www.esa.int/livingplanet/goce/ gives further details and regular updates concerning the evolution of the GOCE mission.)

6. Glossary

Argo: An autonomous global *in-situ* observing system based on an array of up to 3000 profiling floats (when fully implemented) which provides temperature and salinity measurements, typically at depths from 0 to 2000 meters every 10 days. The data are transmitted via ARGOS. In between the 10 days regular ascents they descend back to about 2000 meters where they drift passively with the deep current.
Equipotential surface: A surface where the gravity potential W is a constant. Points on one such surface may be determined regionally with tide-gauges, which define the regional mean sea-level.
Geoid: Equipotential surface which over the ocean approximates the global mean sea-level, i.e., a global set of tide-gauges and levelling benchmarks, after sub-

traction of the dynamic components. It can be considered as the surface of the hypothetical ocean at rest.

Geoid height: The height, N, of a point on the geoid with respect to the ellipsoid (positive upward). The values range from -105 to $+95$ metres, and are associated with long wavelength features (several thousand kilometres). In comparison, variations of shorter scale (tens to hundreds of kilometres) have a magnitude from a few centimetres to one or a few metres.

Geostrophic surface current: The surface current maintained by the balance that is established between the oppositely directed Coriolis force (due to the Earth's rotation) and the surface pressure gradient force. The current is oriented along the isobars, with the high pressure to the right (left) in northern (southern) hemisphere.

Global (geopotential) model: A model of the Earth's gravitational potential in the form of a set of spherical harmonic coefficients, truncated at a maximum degree and order L, so that the maximum resolved half-wavelength, $D = 20{,}000$ km/L.

Gravitational acceleration: The acceleration of a test mass due to the action on it of the gravitational force (mass attraction). Close to the Earth the dominant effect of the gravitational force is due to the mass of the Earth itself. In vacuum the acceleration of a free falling test mass is purely gravitational.

Gravitational field: This is the mathematical function expressing the variation of the action of gravitation in space (or on a surface). In the case of the gravitation force or acceleration vector it is vector field, in the case of the gravitational potential it is a scalar field.

Gravitational potential (V): Potential associated with the attraction of masses.

Gravity: The magnitude, g, of the gradient of W at the Earth's surface and of V in space. It may be observed by an absolute technique (e.g., in a free fall experiment) or relatively (as a difference) by a spring gravimeter. Gravity is expressed in m/s^2 or in milliGal (1 mGal = 10^{-5} m/s^2; 1 Gal = 10^{-2} m/s^2). The mean value of the Earth's *gravity* at the surface is about 981000 mGal (the well-known 9.81 m/s^2); it varies from 978100 mGal at the equator to 983200 mGal to the pole due to the Earth's flattening and rotation.

Gravity anomaly: At any point of given latitude and orthometric height, the gravity anomaly Δg is the value derived by subtracting measured and normal gravity ($\Delta g = g - \gamma$). The normal gravity γ is calculated at a point with the ellipsoidal height put equal to the orthometric height. Gravity anomalies due to density inhomogeneities, mountain ridges, etc., range from tens to hundreds of milliGals.

Gravity gradients: Derivatives of the gravity vector, i.e., second-order derivatives of W at the Earth's surface and of V in space. Certain linear combinations may be measured by a torsion-balance at Earth's surface, and by forming differences of adjacent accelerometer measurements in space. Gravity gradients are expressed in *Eötvös* ($1\,E = 10^{-9}\,s^{-2}$). The largest component is the vertical gravity gradient, being about 3000 E on Earth (gravity changes by 3×10^{-6} m/s^2 per metre of elevation). The horizontal components are approximately half this size; mixed gradients (derivatives in two independent directions) are below 100 E for the nor-

mal field. Gravity-gradient anomalies can be much larger, and can reach 1000 E in mountainous areas.

Gravity potential (W): Referred to the Earth this is the sum of the gravitational potential (V) and of the centrifugal potential (C) of the rotating Earth. Differences between two points may be observed by levelling.

Height datum: This is defined by the equipotential surface which best agrees with local mean sea-level calculated from uniformly distributed tide-gauges for a specific time period.

Kaula's rule: For a given degree, the quadratic mean (over all orders) of the harmonic coefficients for the Earth decreases approximately like $10^{-5}/l^2$; the square of this quantity is called degree variance and corresponds to the signal power spectrum density.

Mean Earth ellipsoid: This is an ellipsoid of revolution, rotating with the Earth around its z-axis, and centred at the Earth's centre of mass. It is determined as the surface which gives the best fit (in some sense) to mean sea-level. The height above this ellipsoid, h, is measured along the normal to the ellipsoid. It is observed indirectly by satellite positioning (such as GPS) from the determined Cartesian co-ordinates (x, y, z).

Meridional overturning: Differences in the heating and cooling of the sea surface as well as salinity changes due to evaporation, precipitation, ice formation, and melting cause density differences, that, in turn, produce currents. At the basin scale (>1000 km) such temporal and spatial differences in salinity and temperature (and hence density) lead to the thermohaline circulation. For instance, in the Atlantic Ocean warm and saline surface water is transported northwards from equator. At high latitudes this water is exposed to strong surface cooling coupled with salt rejection due to sea ice formation that can produce surface water dense enough to sink. Subsequently, this dense water returns southward as a deep flow. This circulation pattern is called the meridional overturning.

Orthometric height: The height, H, measured from the height datum reference equipotential surface (generally parallel to the geoid); this is commonly called the height above mean sea-level. It is observed by levelling; the measurements (level differences and gravity) yield the geopotential number, which is converted to metric units by dividing by the mean gravity along the plumbline. This is how the height system of most countries is established.

Spherical harmonic coefficients: The potential V (or T) may be expanded as an infinite series of spherical harmonic functions (product of Legendre polynomials and cosine/sine functions, see Equation (2.2.1)), which are the spherical equivalent of Fourier series in a plane. The coefficients of the series are numbered according to degree and order, l and m respectively ($m \leq l$), which correspond to wave numbers in the plane. The zonal harmonics are those coefficients of order zero and correspond to averages of the potential in longitude. The other coefficients are called tesseral harmonics (sectorial when $l = m$).

Time-wise approach: The measurable gravity gradients are considered as time series over the whole mission duration along the spacecraft trajectories. The series coefficients are linearly related to the coefficients of a spherical harmonic expansion of maximum degree L. Then the results may be expressed as the standard deviation of $(L + 1)^2$ coefficients. From these error estimates, errors in other quantities may be derived by linear error propagation.

Acknowledgements

Part of the material of this paper is taken from the "Gravity Field and Steady-State Ocean Circulation Mission, Report for Mission Selection, ESA, SP-1233(1), Noordwijk, 1999". In this aspect we are very grateful for the valuable contributions made by O.B. Andersen, A. Anselmi, H. Bassuer, S. Cesare, E. Chassignet, E. Dombrowsky, C. Gerlach, P. Hoyng, J. van den IJssel, R. Klees, R. Koop, P. Knudsen, P-Y. Le Traon, R. Licata, J. Müller, H. Oberndorfer, F. Ponchaut, C. Readings, J. Schröter, A. Selig, M. Smit, L. Vaillon, E. Willemenot and D. J. Wingham. Moreover, the assistance of the technical expert team in the Earth Observation Envelope Program (ESA-ESTEC) including D. Lamarre, D. Muzi, A. Popescu, M. Reynolds and A. Tobias is gratefully acknowledged. Financial support to this work has been obtained from European Space Agency. The first author was also supported by the Norwegian Research Council.

References

Aguirre-Martinez, M. and Cesare, S.: 1999, 'GOCE Mission Concept, Error Derivation and Performances', *Bolletino di Geofisica Teorica ed Applicata* **40**, 295–302.

Aguirre-Martinez, M.: 1999, 'Derivation of the Satellite Gravity Gradient Observables and Recovery of the Centrifugal Terms in GOCE', ESA-ESTEC Working Paper EWP-2033, ESA Publication Division, ESTEC, Noordwijk, The Netherlands.

Arabelos, D. and Tscherning,C. C.: 2001, 'Improvements in Height Datum Transfer Expected from the GOCE Mission', *J. Geodesy* **75**, 308–312.

Balmino, G., Perosanz,F., Rummel, R., Sneeuw, N., and Sünkel, H.: 1999, 'CHAMP, GRACE and GOCE: Mission Concepts and Simulations', *Bollettino di Geofisica Teorica ed Applicata* **40**(3-4), 309–320.

Biancale, R. , Balmino, G., Lemoine, J.-M., Marty, J.-C., Moynot, B., Barlier, F., Exertier, P., Laurain, O., Gegout, P., Schwintzer, P., Reigber, C., Bode, A., König, R., Massmann, F.-H., Raimondo, J.-C., Schmidt, R., and Zhu, S.Y.: 2000, 'A New Global Gravity Field Model from Satellite Orbit Perturbations: GRIM5-S1', *Geophysical Research Letters* **27**(22), 3611–3614.

Bijlsma, L., Ehler, C. N., Klein, R. J. T., Kulshrestha, S. M., McLean, R. F., Mimura, N., Nicholls, R. J., Nurse, L. A., Pérez Nieto, H., Stakhiv, E. Z., Turner, R. K., and Warrick, R. A.: 1996, in R. T. Watson, M. C. Zinyowera, and R. H. Moss (eds.), *Coastal Zones and Small Islands (Chapter 9), In Climate Change 1995: Impacts, Adaptations and Mitigation of Climate Change: Scientific-technical Analysis. Contribution of Working Group II to the Second Assessment Report of the Intergovernmental Panel on Climate Change*, Cambridge University Press, Cambridge, UK, 879 pp.

Bryan, K.: 1996, 'The Steric Component of Sea-level Rise Associated with Enhanced Greenhouse Warming: A Model Study', *Climate Dynamics* **12**, 545–555.

Chassignet, E. P. and Garraffo, Z. D.: 2001, Viscosity parameterisation and the Gulf Stream separation, in P. Muller and D. Hendersen (eds.), *Proceedings Aha Huliko a Hawaiian Winter Workshop: From Stirring to Mixing in a Stratified Ocean*, University of Hawaii, pp. 37–41.

Church, J. A., Gregory, J. M., Huybrechts, P., Kuhn, M., Lambeck, K., Nhuan, M. T., Qin, D., and Woodworth, P. L.: 2001, in J. T. Houghton, Y. Ding, D. J. Griggs, M. Noguer, P. J. van der Linden, X. Dai, K. Maskell and C. A. Johnson (eds.), *Changes in Sea-level (Chapter 11), In Climate Change 2001: The Scientific Basis. Contribution of working group I to the Third Assessment Report of the Intergovernmental Panel on Climate Change*, Cambridge University Press, Cambridge, UK.

Di Donato G., Negredo, A.M., Sabadini, R and Vermeersen, L.L.A.: 1999, 'Multiple Processes Causing Sea-level Rise in the Central Mediterranean', *Geophys. Res. Letters* **26**(12), 1769–1772.

Di Donato, G., Vermeersen, L. L. A., and Sabadini, R.: 2000, 'Sea-level Changes, Geoid and Gravity Anomalies Due to Pleistocene Deglaciation by Means of Multilayered Analytical Earth Models', *Tectonophysics* **320**, 409–418.

Drinkwater, M. R., Floberghagen, R., Haagmans, R., Muzi, D., and Popescu, A.: 2003, 'GOCE: ESA's first Earth Explorer Core Mission', in G. B. Beutler, M. R. Drinkwater, R. Rummel, and R. von Steiger (eds.), *Earth Gravity Field from Space – from Sensors to Earth Sciences*, Space Sciences Series of ISSI, Vol. 18, pp. 419–433, Kluwer Academic Publishers, Dordrecht, Netherlands.

Dziewonski, A. M. and Anderson, D. L.: 1981, 'Preliminary Reference Earth Model', *Phys. Earth Planet. Int.* **25**, 297–356.

ESA, Reports for Mission Selection: 1999, *Gravity Field and Steady-State Ocean Circulation Mission*, SP-1233(1), ESA Publication Division, ESTEC, Noordwijk, The Netherlands (available from web site http://www.esa.int/livingplanet/goce).

Forsberg, R.: 1985, 'Gravity-induced Position Errors in Inertial Surveying', in *Proc. Inertial Technology for Surveying and Geodesy*, Banff, Canada.

Ganachaud, A., Wunsch, C., Kim, M-C., and Tapley, B.: 1997, 'Combination of TOPEX/Poseidon Data with a Hydrographic Inversion for Determination of the Oceanic General Circulation', *Geophys. J. Int.* **128**, 708–722.

Gill, A. E.: 1982, *Atmosphere – Ocean Dynamics*, Academic Press, New York, 662 pp.

GRACE – Gravity Recovery and Climate Experiment: 1998, 'Science and Mission Requirements Document, Revision A', *JPLD-15928*, NASA's Earth System Science Pathfinder Program.

Heck, B. and Rummel, R.: 1990, 'Strategies for Solving the Vertical Datum Problem using Terrestrial and Satellite Geodetic Sata', in H. Sünkel and T. Baker (eds.), *Sea-surface Topography and Geoid*, Springer, Berlin, pp. 116–128.

Heiskanen, W. A. and Moritz, H.: 1967, *Physical Geodesy*, Freeman, San Francisco.

Hughes, C. W. and Ash, E.: 2001, 'Eddy Forcing of the Mean Flow in the Southern Ocean', *J. Geophys. Res. Ocean* **106**(C2), 2713–2722.

Kaula W. M.: 1996, *Theory of Satellite Geodesy*, Waltham, Blaisdell.

Khafid: 1998, *On the Unification of Indonesian Local Heights*, DGK, C-488, München.

LeGrand, P. and Minster, J.-F.: 1999, 'Impact of the GOCE Gravity Mission on Ocean Circulation Estimates', *Geophysical Research Letters* **26**(13), 1881–1884.

LeGrand, P.: 2001, 'Impact of the Gravity Field and Steady-State Ocean Explorer (GOCE) Mission on Ocean Circulation Estimates. Volume Fluxes in Climatological Inverse Model of the Atlantic', *J. Geophys. Res. Ocean* **106**, 19597–19610.

Lemoine, F. G., Kenyon, S. C., Factor, J. K., Trimmer, R. G., Pavlis, N. K., Chinn, D. S., Cox, C. M., Klosko, S. M., Luthcke, S. B., Torrence, M. H., Wang, Y. M., Williamson, R. G., Pavlis, E. C., Rapp, R. H., and Olson, T. R.: 1998, 'The Development of the Joint NASA GSFC and the National Imagery and Mapping Agency (NIMA) Geopotential Model EGM96', National

Aeronautics and Space Administration Report, NASA/TP-1998-206861, Goddard Space Flight Center, Greenbelt, MD.

Le Provost C., LeGrand, P., Dombrowsky, E., Le Traon, P. Y., Losch, M., Ponchaut, F., Schröter, J., Sloyan, B., and Sneeuw, N.: 1999, 'Impact of GOCE for Ocean Circulation Studies', Final Report, ESA study contract 13175/98/NL/GD.

McKenzie, D.: 1994, 'Relationship between Topography and Gravity on Earth and Venus' *Icarus* **112**, 55–88.

Negredo, A. M., Carminati, E., Barba, S., and Sabadini, R.: 1999, 'Dynamic Modelling of Stress Accumulation in Central Italy', *Geophys. Res. Letters* **26**(13), 1945–1948.

NRC: 1997, *Satellite Gravity and Geosphere*, National Academy Press, Washington, D.C.

Oberndorfer, H. Müller, J., Dorobantu, R., Gerlach, C., Rummel, R., Sneeuw, N., Koop, R., Visser, P., Hoyng, P., Selig, A., and Smit, M.: 2000, Simulation of the GOCE Gravity Field Mission, in R. Rummel, H. Drewes, W. Bosch, and H Hornik (eds.), *Towards an Integrated Global Geodetic Observing System (IGGOS)*, IAG symposium 120, Springer, pp. 201–204.

Paiva, A. M., Hargrove, J. T., Chassignet, E. P., and Bleck, R.: 1999, 'Turbulent Behaviour of a Fine Mesh (1/12 Degree) Numerical Simulation of the North Atlantic', *J. Marine Systems* **21**, 307–320.

Peltier, W. R.: 1998, 'Postglacial Variations in the Level of the Sea: Implications for Climate Dynamics and Solid-Earth Geophysics', *Reviews of Geophysics* **36**(4), 603–689.

Reigber Ch., Bock, R., C., Forste, Grunwaldt, L., Jakowski, N., Lühr, H., Schwintzer, P., and Tilgner, C.: 1996, *CHAMP Phase-B Executive Summary*, G.F.Z., STR96/13.

Roemmich, D. and Owens, W. B.: 2000, 'The Argo Project: Global Ocean Observations for Understanding and Prediction of Climate Variability', *Oceanography* **13**, 45–50.

Rosborough, G. W.: 1987, 'Radial, Transverse and Normal Satellite Position Perturbations Due to the Geopotential', *Celestial Mechanics* **40**, 409–421.

Rummel, R.: 1992, 'GPS, Heights and the Role of the Geoid', *Geodetical Info Magazine* **6**(8), 52–56.

Rummel, R. Balmino, G., Johannessen, J. A., Visser, P., and Woodworth, P. L.: 2002, 'Dedicated Gravity Field Missions – Principles and Aims', *J. Geodynamics* **33**, 3–20.

Schröter, J., Losch, M., and Sloyan, B.: 2002, 'Impact of the Gravity field and Steady-state Ocean Circulation Explorer (GOCE) Mission on Ocean Circulation Estimates: 2. Volume and Heat Fluxes across Hydrographic Sections of Unequally Spaced Stations', *J. Geophys. Res.* **107**(C2).

Schwarz, K. P.: 1981, *Gravity Induced Position Errors in Airborne Inertial Navigation*, The Ohio State University, Columbus, Ohio, p. 326.

Schwarz, K. P. and Sideris, M. G.: 1987, 'Orthometric Heights without Levelling', *J. Surv. Engineering* **113**(1), 28.

Schwintzer, P., Reigber, C., Bode, A., Kang, Z., Zhu, S. Y., Massmann, F. H., Raimondo, J. C., Biancale, R., Balmino, G., Lemoine, J. M., Moynot, B., Marty, J. C., Barlier, F., and Boudon, Y.: 1997, 'Long-wavelength Global Gravity Field Models: GRIM4-S4, GRIM-C4', *J. Geodesy* **71**(4), 189–208.

SID: 2000, *GOCE End-to-End Closed Loop Simulation*, Final Report, ESTEC study contract 12735/98/NL/GD.

Sneeuw, N.: 1992, 'Representation Coefficients and their Use in Satellite Geodesy', *Manuscripta Geodetica* **17**, 117–123.

Sünkel H., Rummel, R., Klees, R., Ilk, K. H., Sabadini, R., Tscherning, C. C., and Sanso, F.: 2000, *From Eotvös to mGal*, Final Report, ESA study contract, ESTEC, No. 13392/98/NL/GD.

Touboul, P., Willemenot, E., Foulon, B., and Josselin, V.: 1999, 'Accelerometers for CHAMP, GRACE and GOCE Space Missions: Synergy and Evolution', *Bolletino di Geofisica Teorica ed Applicata* **40**, 321–327.

Tscherning, C. C., Sabadini, R., Andersen, O., Arabelos, D., Carminati, E., Forsberg, R., Knudsen, P., Larsen, J., and Strykowski, G.: 1999, *Refinement of the Current Observation Requirements for GOCE*, Final Report, ESA study contract 13229/98/NL/GD.

Tushingham, A. M., and Peltier, W. P.: 1991, 'ICE-3G: A New Global Model of Late Pleistocene Deglaciation Based upon Geophysical Predictions of Postglacial Relative Sea-level Change', *J. Geophys. Res.* **96**, 4497–4523.

Vermeersen, L. L. A. and Sabadini, R.: 1997, 'A New Class of Stratified Viscoelastic Models by Analytical Techniques', *Geophys. J. Int.* **129**, 531–570.

Visser, P. N. A. M. and van den IJssel, J.: 2000, 'GPS-based Precise Orbit Determination of the Very Low Earth Orbiting Gravity Mission GOCE', *J .Geodesy* **74**(7/8), 590–602.

Visser, P. N. A. M., Rummel, R., Balmino, G., Sünkel, H., Johannessen, J. A., Aquirre, M., Woodworth, P. L., Le Provost, C., Tscherning, C. C., and Sabadini, R.: 2002, 'The European Earth Explorer Mission GOCE: Impact for the Geosciences, Ice Sheets, Sea-level and the Dynamic Earth', in J. Mitrovica and L. L. A. Vermeersen (eds.), *Geodynamics Series 29*, American Geophysical Union, pp. 95–107.

Wahr, J. M., Jayne, S. R., and Bryan, F. O.: 2002, 'A Method of Inferring Changes in Deep Ocean Currents from Satellite Measurements of Time-varying Gravity', *J. Geophys. Res. Ocean* **107**.

Warrick, R. A., Le Provost, C., Meier, M. F., Oerlemans, J., and Woodworth, P. L.: 1996, Changes in Sea-level (Chapter 7), in J. T. Houghton, L. G. Meira Filho, B. A. Callander, N. Harris, A. Kattenberg, and K. Maskell (eds.), *Climate Change 1995: The Science of Climate Change. Contribution of Working Group I to the Second Assessment Report of the Intergovernmental Panel on Climate Change*, Cambridge University Press, Cambridge, UK, 572 pp.

Woodworth, P., Johannessen, J. A., LeGrand, P., Le Provost, C., Balmino, G., Rummel, R., Sabadini, R., Sünkel, H., Tscherning, C. C., and Visser, P. N. A. M.: 1998, 'Towards the Definitive Space Gravity Mission', *International WOCE Newsletter* **33**, 37–40.

Wunsch, C. and Stammer, D.: 1998, 'Satellite Altimetry, the Marine Geoid, and the Oceanic General Circulation', *Annual Reviews of Earth and Planetary Science*, **26**, 219–253.

Xu, P. and Rummel, R.: 1991, *A Quality Investigation of Global Vertical Datum Connection*, Netherlands Geodetic Commision, 34, Delft, The Netherlands.

Zerbini, S., Achache, J., Anderson, A. J., Arnet, F., Geiger, A., Klingelé, E., Sabadini, R., and Tinte, S.: 1992, *Study of the Geophysical Impact of High-resolution Earth Potential Fields Information*, Final Report, ESA Study contract.